Elsevier Editorial System(tm) for Geomorphology

Manuscript Draft

Manuscript Number: GEOMOR-6270R2

Title: Morphological changes, beach inundation and overwash caused by an extreme storm on a low-lying embayed beach bounded by a dune system (NW Mediterranean)

Article Type: Research Paper

Keywords: LiDAR; vulnerability; shoreline erosion and accretion; sediment budget.

Corresponding Author: Ms. Ruth Durán,

Corresponding Author's Institution: Instituto de Ciencias del Mar (CSIC)

First Author: Ruth Durán

Order of Authors: Ruth Durán; Jorge Guillén; Antonio Ruiz; José A Jiménez; Enric Sagristà

Abstract: The geomorphological evolution of a low-lying, micro-tidal sandy beach in the western Mediterranean, the Pals beach, was characterized using airborne Light Detection and Ranging (LiDAR) data. Data were collected in prior to, and six months after, the impact of an extreme storm with a return period of 50 years with the aim of characterizing the beach's response to the storm. The use of repeated high-resolution topographic data to quantify beach geomorphic changes has allowed assessing the accuracy of different proxies for estimating beach volume changes. Results revealed that changes in the shoreline position cannot accurately reproduce beach volume changes in low-lying beaches where overwash processes are significant. Observations also suggested that volume estimations from beach profiles do not accurately represent subaerial volume changes at large profile distances in beaches with significant alongshore geomorphological variability. Accordingly, the segmentation of the beach into regularly spaced bins is proposed to assess alongshore variations in the beach volume with the accuracy of the topographic data.
The morphological evolution of Pals beach during the study period showed a net shoreline retreat (-4 m) and a significant sediment gain on the subaerial beach (+7.5 m3/m). The net gain of sediment is mostly due to the impact of the extreme storm, driving significant overwash processes that transport sediment landwards, increasing volume on the backshore and dunes. The increase of volume on the foreshore and the presence of cuspate morphologies along the shoreline also evidence post-storm beach recovery. Observed morphological changes exhibit a high variability along the beach related to variations in the beach morphology. Changes in the morphology and migration of megacusps result in a high variability in the shoreline position and foreshore volume changes. On the other hand, larger morphological changes on the backshore and larger inundation distances occur when the beach and the dunes are lower, favouring the dominance of overwash. The observed storm-induced morphological changes differ from predicted beach storm impacts because of spatial and temporal variations in the beach morphology, suggesting that detailed

morphological parameters and indicators used for predicting beach vulnerability to storms should be regularly updated in order to represent the pre-storm beach conditions. Finally, observed morphological changes in the Pals Bay evidenced a different behaviour between natural and urban areas, with better post-storm beach recovery on natural areas where the beach is not artificially narrowed.

Highlights

LiDAR data are used to evaluate different proxies for estimating beach volume changes.

Overwash during severe storms increases the subaerial beach volume.

Accurate and updated morphological data improves assessment of potential inundation.

Anthropogenic intervention on the beach reduces post-storm beach recovery.

Morphological changes, beach inundation and overwash caused by an extreme storm on a low-lying embayed beach bounded by a dune system (NW Mediterranean)

Ruth Durán[1], Jorge Guillén[1], Antonio Ruiz[2], José A. Jiménez[3], Enric Sagristà[1]

[1] Institut de Ciències del Mar (CSIC), Passeig Marítim de la Barceloneta 37-49, 08003 Barcelona, Spain. E-mail: rduran@icm.csic.es

[2] Institut Cartogràfic i Geològic de Catalunya, Parc de Montjuïc, 08038 Barcelona, Spain.

[3] Laboratori d'Enginyeria Marítima, Universitat Politècnica de Catalunya·BarcelonaTech, Campus Nord - Ed. D1, c/ Jordi Girona 1-3, 08034 Barcelona, Spain.

Abstract

The geomorphological evolution of a low-lying, micro-tidal sandy beach in the western Mediterranean, Pals beach, was characterized using airborne Light Detection and Ranging (LiDAR) data. Data were collected in prior to and six months after the impact of an extreme storm with a return period of approx. 50 years, with the aim of characterizing the beach's response to the storm. The use of repeated high-resolution topographic data to quantify beach geomorphic changes has allowed assessment of the accuracy of different proxies for estimating beach volume changes. Results revealed that changes in the shoreline position cannot accurately reproduce beach volume changes on low-lying beaches where overwash processes are significant. Observations also suggested that volume estimations from beach profiles do not accurately represent subaerial volume changes at large profile distances on beaches with significant alongshore geomorphological variability. Accordingly, the segmentation of the beach into regularly spaced bins is proposed to assess alongshore variations in the beach volume with the accuracy of the topographic data. The morphological evolution of Pals beach during the study period showed a net shoreline retreat (-4 m) and a significant sediment gain on the subaerial beach (+7.5 m^3/m). The net gain of sediment is mostly due to the impact of the extreme storm, driving significant overwash processes that transport sediment landwards,

increasing volume on the backshore and dunes. The increase of volume on the foreshore and the presence of cuspate morphologies along the shoreline also evidence post-storm beach recovery. Observed morphological changes exhibit a high variability along the beach related to variations in beach morphology. Changes in the morphology and migration of megacusps result in a high variability in the shoreline position and foreshore volume changes. On the other hand, larger morphological changes on the backshore and larger inundation distances occur when the beach and the dunes are lower, favouring the dominance of overwash. The observed storm-induced morphological changes differ from predicted beach storm impacts because of spatial and temporal variations in the beach morphology, suggesting that detailed morphological parameters and indicators used for predicting beach vulnerability to storms should be regularly updated in order to represent the pre-storm beach conditions. Finally, observed morphological changes in Pals Bay evidenced a different behaviour between natural and urban areas, with better post-storm beach recovery on natural areas where the beach is not artificially narrowed.

Keywords: LiDAR, vulnerability, shoreline erosion and accretion, sediment budget.

1. Introduction

Understanding how low-lying coasts respond to storms is crucial for assessing the vulnerability of these areas to natural hazards and developing tools and management approaches to reduce risk and increase coastal resilience. Low-lying coasts are highly sensitive to storm-induced hazards such as beach erosion, breaching of the dune system, overwash and inundation (e.g. Sallenger, 2000; Morton, 2002). Furthermore, human activities such as flow regulation of river systems, coastal construction and tourism add additional pressure on the coastal system by increasing vulnerability in already highly vulnerable areas (Morton et al., 1994; Willis and Griggs, 2003; Richter et al., 2013). In relation to climate change, low-lying coasts are particularly vulnerable because of rising sea levels and accelerated coastal erosion (Nicholls et

al., 2014). Sea-level rise will raise storm-induced maximum water levels (Fiore et al., 2009), enhancing the impact of storms by increasing the potential for erosion and coastal flooding (Zhang et al., 2002). Assessing vulnerability to inundation of these areas by identifying coastal areas at risk of flooding and defining flood extent is therefore a key issue at both European and global level. In Europe, the assessment of flood risks is dealt with in the European Flooding Directive 2007/60/EC and the Protocol of Integrated Coastal Zone Management (PAP/RAC, 2007).

The vulnerability of a coast to inundation during storms depends on the morphology of the beach and dune relative to the intensity of the ocean's forcing (Wright and Short, 1984; Sallenger, 2000). Even in the context of steady forcing, some areas of the beach may experience severe erosion and/or overwash while adjacent areas may appear unaffected, mostly due to the spatial variability of the beach width and slope, or the dune elevation (Sallenger et al., 2003; Stockdon et al., 2007). Recent studies have found that foredune accretion is dominant in wider and low-gradient beaches while eroding dunes are associated with narrower, steeper beaches (Saye et al., 2005; Keijpers et al., 2014). Similarly, small variations in the elevation, volume and alongshore extent of the foredune also lead to a more spatially variable beach response to storms (Sallenger, 2000; Houser et al., 2008, 2015). In locations where storm-induced water levels exceed the crest of the dune or the dune is breached, sediment is transported landward as overwash and deposited on the backdunes (Sallenger, 2000; Stockdon et al., 2007; de Vries et al., 2008). The detailed assessment of the magnitude and alongshore variability of the beach response to storms is therefore required to accurately predict the coastal response to storms and to identify areas at risk of erosion and flooding.

Remote sensing techniques such as airborne laser altimetry (LiDAR) are now commonly used to quantify storm-induced morphological changes and post-storm beach recovery (e.g. Zhang et al., 2005; Stockdon et al., 2009; Keijpers et al., 2014; among others). LiDAR technology provides elevation data with high vertical accuracy (less than 20 cm) and horizontal resolution (about 50 cm), high point density and large coverage areas (~400 m of swath wide), which

resolve the small-scale variability of the beach and dune morphology for an accurate assessment of coastal vulnerability during storms (Sallenger et al., 2003). In addition, the highly automated aspect of LiDAR collection lends itself to resampling areas quickly and efficiently, which is particularly important in the coastal zone, where storm-induced changes can be dramatic and rapid.

The aim of this paper is to characterize and quantify the impact of an 'extreme' storm and the post-storm recovery of a large bay on the NW Mediterranean coast, Pals Bay, using LiDAR-derived topographic data collected prior to and six months after the storm. The morphological evolution of the backshore during the study period is primarily due to the extreme storm. Conversely, the recorded changes in the foreshore are also influenced by other storms of smaller magnitude, as well as the post-storm beach recovery. Thus, only morphological changes occurred at elevations higher than the maximum storm-induced water during the moderate storms are associated to the impact of the extreme storm. More specifically, this work aims to: (i) evaluate the beach's response to the impact of the storm by characterizing morphological changes between both surveys; (ii) quantify the maximum observed inundation and compare it with predicted vulnerability to storm-induced inundation; and (iii) assess the anthropogenic influence on the beach response.

2. Field site

Pals Bay, on the northern coast of Catalonia (NW Mediterranean), is a low topographic coast bounded by two rocky headlands, the Montgrí massif to the north and Cape Begur to the south (Fig. 1A). It belongs to the Baix Empordà littoral plain, which includes extensive marshes, river channels, a complex dune system, urbanized areas such as L'Estartit, Els Griells, El Mas Pinell and Pals beach golf course, and embayed beaches (Figs. 1B, 1C). Much of the littoral plain is currently considered a protected area at regional and European levels because of its great natural value (Fig. 1B).

Two rivers flow into Pals Bay: the Ter River, which is 212 km long and has a draining area of about 3000 km^2, and the Daro River, which is 35 km long and has a drainage area of 300 km^2 (Fig. 1A) (ACA, 2002; Liquete et al., 2009). These rivers have a typical Mediterranean torrential regime, with most of the discharge concentrated in short-lived flood events, particularly between December and February (Sabater et al., 1992; Liquete et al., 2009). During the study period, the highest river flow (120 $m^3 s^{-1}$ in the Ter River and 7.6 $m^3 s^{-1}$ in the Daro River) was recorded on 26 December 2008 and was associated with heavy rainfall of up to 3.36 mm h^{-1} recorded by the Girona rain gauge (Fig. 2). Changes in the course of these rivers together with the local geomorphology and anthropogenic activities played an important role in the formation and evolution of the Baix Empordà dune system (Cros and Serra, 1993). The main changes in the Ter River course have occurred during the last millennium as a result of periods of high fluvial activity, widespread deforestation and accelerated sedimentation (Marqués and Julià, 2005). The main course of the Ter River frequently changed along two active channels from a river bifurcation at the Verges site (Montaner et al., 2010). The northern branch flowed into the Roses Bay, contributing to the sedimentary infill of the Alt Empordà littoral plain and acting as a natural barrier to the sediment transported by northern winds (Fig. 1B). In the early 14^{th} century AD, the avulsion of the Ter River at Verges produced the abandonment of the northern branch in favour of the eastern course (Montaner Roviras and Solà Subiranas, 2004), contributing to the progressive infill of the Baix Empordà plain and the formation of the Baix Empordà dune system (Marqués and Llulià, 2005). At present, the configuration of the dune system is controlled by the strong northern winds, the west-east orientation of the main river courses and the presence of local topographic highs such as the Montgrí massif and Cape Begur, which act as natural barriers against aeolian processes (Fig. 1B).

Pals Bay is characterized by a large sandy beach, named hereafter Pals beach, and two small pocket beaches, Illa Roja and Sa Riera (Fig. 1B). Pals beach is a typical embayed beach extending 6800 m from L'Estartit to Cape Begur (Fig. 1B). The beach width is highly variable alongshore between 25 m at Els Griells and 130 m in the south (Fig. 1C). Sediment grain size

shows high spatial variability, with a median grain size (d50) ranging between 230 μm in the north and 1260 μm in the south (CIIRC, 2010). This trend in the grain is reflected in the beach slope and the berm height, which also increases southward from 1.3 m at L'Estartit to 2.7-3.2 m in the southernmost sector of the beach (CIIRC, 2010). Pals beach is backed by a discontinuous vegetated foredune that covers an area of 205,000 m^2, with a predominant NNW-SSE orientation. The dunes show a variable height along the beach, varying from 0.5-1.5 m in the north to 3.5 m in the south. Illa Roja and Sa Riera are small pocket beaches located in the southern part of Pals Bay and bounded by 45 m-high cliffs (Fig. 1B). Illa Roja has a length of 185 m, a variable width (8-35 m), and a mean grain size of 1670 μm. Sa Riera has a length of 186 m, a variable width (50-95 m), and a mean grain size of 1770 μm (CIIRC, 2010).

Pals Bay is a microtidal environment with a tidal range of about 0.2 m. Dominant winds in the area are from the north and northwest in December and January and from the south and east in February, March, April and November. High velocities have been recorded for marine winds (E winds) during storm conditions associated with cyclonic activity over the NW Mediterranean (Font, 1990). Wave climate in the region is highly seasonal, with the severest conditions usually occurring from late autumn to early spring (Bolaños et al., 2009). Statistical analysis of wave conditions in the region showed a yearly mean significant wave height (H_s) of 0.77 m with a maximum H_s of 7.8 m (Mendoza et al., 2011). Storms with H_s between 3.5 and 4.25 m are the most frequent, but severe events (H_s up to 5) and even extreme events (H_s higher than 5 m) are also recorded. Severe and extreme storms have a predominant easterly direction, whereas less energetic storms arrive from the south (Mendoza et al., 2011).

3. Data sets and methods

3.1 Storm-induced water levels

Storm-induced water levels (R_{low} and R_{high}) were calculated to characterize fluid forcing during the study period, and particularly at the peak of the extreme storm. R_{low} is the sum of the astronomical tide, storm surge and wave-induced setup (η), as proposed by Stockdon et al.

(2007) (Fig. 3). R_{high} represents the highest elevation of the landward margin of swash relative to a fixed vertical datum. It includes the combined effects of the astronomical tide, storm surge and the wave-induced runup ($R_{2\%}$) (Sallenger, 2000; Stockdon et al., 2007) (Fig. 3). The elevation of $R_{2\%}$ was calculated from offshore wave conditions using Stockdon's empirical parametrization (Stockdon et al., 2006), which includes both wave-induced setup and swash and is given by

$$R_{2\%} = 1.1\left(0.35\beta_f\sqrt{H_s 1.56T_p^2} + \frac{\sqrt{\left[H_s 1.56T_p^2\left(0.563\beta_f^2+0.004\right)\right]}}{2}\right), \quad (1)$$

where β_f is the foreshore slope, defined as the average slope over the portion of the beach extending from the shoreline to the crest berm, H_s is the significant wave height, and T_p the associated peak period.

R_{high} was calculated over the study period considering the mean foreshore slope of the beach (β_f = 0.11 ± 0.03) to characterized the storms occurring during the study period, and particularly the most energetic storm. To assess the spatially variable coastal response and to compared it with the storm-impact scaling model presented by Sallenger (2000), the foreshore slope (β_f) and storm-induced extreme water levels (R_{low} and R_{high}) were also calculated along the beach from cross-shore profiles evenly spaced (1 m) in the alongshore direction, considering three different wave conditions: calm weather, the extreme storm and other moderate storms that occurred during the study period.

Still water levels (WL) were derived from tide gauge records (every 2 hours) at L'Estartit harbour (Fig. 1B). It includes both astronomical tide and storm surge. Wave data were recorded by the Palamós wave buoy (Puertos del Estado, www.puertos.es), which is located approximately 4.5 km offshore, at 90 m depth (Fig. 1A). The Palamós wave buoy has been operated since the end of the 1980s, recoding data every hour. The data used in this study include significant wave height (H_s) and peak period (T_p) calculated for 24 minute recordings taken every hour, with a sampling frequency of 4 Hz.

3.2 LiDAR data

Morphological changes in the study area were quantified using LiDAR-derived beach topography complemented with high-resolution (0.25 m) orthophotos acquired on May 2008 and August 2009. Surveys of beach topography were carried out on 16 October 2008 and 11 August 2009 using a Leica ALS50-II airborne laser scanning system. LiDAR uses a laser beam to depict the shape of the terrain. Through a combined use of a laser transmitter with high repeating pulse frequency and a high speed scanning system, very dense measurements of range from the LiDAR system to the terrain surface are produced (Table 1). The global positioning system (GPS) and inertial navigation systems on board allowed 3D position coordinates to be assigned to the points where the signal was reflected. The European Terrestrial Reference System 1989 (ETRS 1989) was used and points were projected to the Universal Transverse Mercator system (zone 31 N). The GRS80 ellipsoidal heights were transformed into orthometric heights by adding the geoid undulations of the local geoid EGM08D595, which is an adaptation of the EGM2008 geoid to the local levelling network (Grau et al., 2012).

The LiDAR points are affected by systematic errors. The main error contribution is a height offset, which we assumed to be constant and different for each strip. It was corrected in a strip adjustment using control fields and LiDAR strips from a previous project, which minimized the height differences in crossing areas as well as the differences between strips and measurements taken in the control fields, following the procedure described in Kornus and Ruiz (2003). The systematic errors for both surveys were simultaneously minimized by least squares. After adjustment, LiDAR point data were classified into ground and non-ground points with TerraScan and TerraModeler from Terrasolid. Finally, high-resolution digital elevation models (DEMs) with a 1-m grid step were interpolated from the points classified as ground, also with the help of TerraModeler. This is an interpolation on flat triangles of a triangulated irregular network model. The absolute height accuracy of the LiDAR points was evaluated in a control field. A flat area without vegetation or other obstructions was chosen. A total of 54 points were measured in the control field with GPS-RTK, which has a vertical precision of 2-3 cm. The

results of the comparison are shown in Table 2. In addition, the relative height accuracy for the temporal coastal change and vertical offsets were quantified from 50 control fields selected from stable flat and hard surfaces adjacent to the beach, as proposed by Zhang et al. (2005). The relative elevation accuracy between the two flights was examined by comparing the elevations of each point within these control fields extracted from the 1-m gridded DEMs. Results revealed a mean difference in elevation of -0.006 ± 0.045, with a root mean square of 0.04 m, lower than the resolution of LiDAR data, thus supporting that no significant errors exist between the two surveys.

3.3 Morphological analysis

3.3.1 Shoreline changes

Topographic data were integrated in the ArcGIS 10.1 Geographical Information System to quantify changes in the shoreline position and subaerial beach volume. The shoreline was defined for each survey as the horizontal position of the datum-based mean high water (Stockdon et al., 2002). The shoreline displacement was calculated as the difference between the initial and final configurations in cross-shore transects at a 1 m intervals along the coast.

To identify changes in the beach planform and to exclude the effect of smaller-scale morphologies (e.g. megacusps), the method proposed by Sancho-García et al. (2013) was applied. In this procedure, the embayed beach is described mathematically by fitting a hyperbolic tangent shape to it (Moreno and Kraus, 1999). The overall beach planform changes are defined as the difference between the initial and final fitted shorelines, whereas residuals provide information about smaller-scale morphologies along the shoreline.

3.3.2 Volume changes

Total volumetric change was calculated by subtracting the DEMs obtained for each survey. The net volumetric change was normalized by the linear metre of coastline (in m^3/m) to compare the differences between the three beaches. To assess cross-shore variations in the subaerial beach

volume, the beach was divided into two sectors: the foreshore, defined between the shoreline and the berm crest, and the backshore, which includes the backshore and the dune system and extends from the berm crest to the landward limit of the observed changes in beach elevation during the study period (Fig. 3).

Alongshore variations in the beach volume changes are commonly quantified by analysing beach profiles along the coast, which essentially consists in reducing 3D topographic data to 2D cross-shore transects (Stockdon et al., 2009; Keijpers et al., 2014). However, previous studies have highlighted that the accuracy of volumetric change measurements from beach transects decreases as the profile spacing increases, particularly on beaches with complex morphology and at short (yearly) timescales (Wright and Short, 1984; Robertson et al., 2007; Muñoz-Perez et al., 2012). Furthermore, the location of the selected profiles can also lead to errors in the beach volume measurements (Pearre and Pauleo, 2009; Theuerkauf and Rodriguez, 2012, 2014). In this work, alongshore variations in the subaerial beach volume changes were quantified by segmenting each DEM into 3D cross-shore segments (called bins) with regular width. The use of bins instead of transects resolves the spatial variability of the beach morphology with the accuracy of the high-resolution topographic data.

To define an appropriate bin width that accurately resolves the spatial variability of the beach morphology, the subaerial beach volume change was calculated from DEM subtraction as well as from beach transects. Different computations were tested by varying profile spacing (from 1 to 200 m, every 5 m) and location (10 different profile locations). The relative volume error was calculated from difference between the net volumes calculated from transects and that obtained for each DEM.

Volume change is calculated for each transect using Equation (2)

$$\Delta V = \sum_{i=1}^{n} Y\, \Delta Z i (X_{i+1} - X_i) \quad (2)$$

where Y is the transect spacing, (X_{i+1}-X_i) is the across-beach distance between grid cells, ΔZ is the change in elevation, and n is the total number of grid cells of each transect.

Results revealed that the best accuracy of beach volume change is achieved from 1 m-spaced profiles, corresponding to the grid resolution (Fig. 4). The accuracy decreases with increasing profile spacing, particularly at distances greater than 20 m. Furthermore, large errors in the beach volume (either over- or under-estimation) appear to be associated with changes in the transect location, regardless of the distance between transects, due to the spatial variability of the beach morphology (Fig. 4). Based on these observations, a bin width of 20 m is considered to represent the observed alongshore variable beach morphology.

3.3.3 Beach vulnerability to inundation

The vulnerability of the beach to inundation during storms was estimated by comparing pre-storm beach morphology (D_{low} and D_{high}) with maximum storm-induced water levels (R_{low} and R_{high}) calculated at the peak of the extreme storm, using the conceptual model proposed by Sallenger (2000) and expanded by Stockdon et al. (2007). D_{high} is the elevation of the dune crest or, in the absence of dunes, the elevation of the beach berm (Fig. 3). D_{low} is defined as the elevation of the base of the dune (Fig. 3). When a dune is not present, D_{low} is not defined. The position of the dune crest and toe were extracted from the 1 m-gridded DEM (and related products such as slope and aspect maps) obtained in the first survey. Where dunes were not present, the berm crest was digitized as the highest position on the beach. After digitization of the position of the dune or berm crest on the DEM, their precise cross-shore location and elevation were automatically identified as the highest elevation within a 5 m-wide swath centred on the digitized line. Where dunes were present, the horizontal position and elevation of the dune base were calculated as the location of maximum slope change within a region (6 m wide) around a line digitized along the dune toe. The location of the dune or berm crest and dune toe was superimposed on the 1 m-spaced cross-shore profiles to verify the accuracy of the elevations extracted from the DEM.

According to Sallenger's model (Sallenger, 2000), swash regime occurs when R_{high} is confined to the foreshore region, collision regime occurs when R_{high} exceeds the base of the dune, and overwash regime occurs when R_{high} equals or exceeds the dune crest. The most extreme regime,

inundation, occurs when R_{low} exceeds the crest of the dune, and the beach and dunes are completely and continually subaqueous. The storm-impact regime was predicted every 1 m along the coast using measurements of pre-storm dune elevation and estimates of storm-induced expected water levels. Results were represented in the figures using a low-pass filter for 20 m length scale in order to represent the observed alongshore variable beach morphology, allowing patterns to be easily identified.

4. Results

4.1 Forcing conditions

Time series of the main forcings in the study area during the study period are illustrated in Fig. 5. Recorded waves show typical climatic conditions of the area, with a stormy period from November 2008 to April 2009 followed by a fair-weather period from May to August 2009 (Figs. 5A, 5B). Following Ojeda and Guillén (2008), significant storms were defined by H_s higher than 2.5 m at the peak of the storm and a minimum duration of 12 h, with H_s higher than 1.5 m. If the interval between two consecutive storms was shorter than 12 h, they were considered as a single double-peaked storm, as was proposed by Mendoza and Jiménez (2009). According to these criteria, six storms impacted the area during the study period (Table 3).

The most energetic storm occurred on 26 December 2008. It was characterized by a H_s of 7.5 m and an associated T_p of 12.2 s at the peak of the storm, with a predominant easterly direction, which induced a maximum water level, R_{high}, of 4.1 ± 1.1 m (Fig. 5D). The magnitude of the astronomical tide and the storm surge recorded by the tidal gauging (0.4 m) was much lower than the wave-induced runup (3.7 m), which constituted the main contributor to increased water levels at the coast during the storm. The storm corresponded to category-V (extreme storm), following the storm intensity scale for the Catalan Sea proposed by Mendoza et al. (2011) with a return period of approx. 50 years (Bolaños et al., 2009). In addition to the extreme storm, other moderate S and NE storms occurred during this period, with H_s between 2.5 and 3.4 m, an

313 associated T_p of between 8 and 11.1 s, and a mean R_{high} of between 1.6 and 2.5 m (Fig. 5, Table
314 3).

315 **4.2 Shoreline variations and beach volume changes**

316 4.2.1 Pals beach

317 Shoreline displacements along the Pals beach during the study period ranged between –29 m
318 and +40.7 m, with a mean shoreline retreat of -3.9 m that resulted in a reduction of 32 787 m^2 in
319 the beach area (7% of the emerged beach area). Shoreline changes showed a non-uniform
320 alongshore pattern (Fig. 6B), reflecting the influence of the evolution of small-scale
321 morphologies, such as megacusps, on the overall beach planform response.

322 Changes in the overall beach shape were derived by comparing the pre- and post-storm fitted
323 shorelines to the hyperbolic tangent shape (Figs. 6C, 6D). Results showed a good fit (squared
324 correlation, r^2, between the fit and the shoreline of almost 1), except in the northernmost sector
325 of the beach where the curvature of the real shoreline is significantly higher than the fitted
326 shape. The shoreline experienced an overall retreat during the study period, although it was not
327 uniform along the beach. The only area where the beach planform experienced accretion was
328 the southernmost extreme of the beach, where the shoreline advanced up to +45 m. It must be
329 considered that net alongshore sediment transport along the beach is towards the south and this
330 area is therefore a typical accumulation zone.

331 Residuals of the fitted shoreline result in secondary morphological features showing two spatial
332 scales (Figs. 6D, 6E): megacusps with a mean spacing of 290 m and amplitudes of 10-15 m and
333 larger rhythmic morphologies with a spacing of up to 2700 m and amplitudes of 75-80 m.
334 Changes in the morphology (amplitude and/or extension) and migration of megacusps produce a
335 differential erosion/accretion pattern along the beach that results in a high variability in the
336 shoreline position (Fig. 6B). The largest rhythmic morphologies also change in amplitude and
337 extension and migrate southward over the study period, particularly in the southern sector of the
338 beach.

In terms of volume, Pals beach experienced a significant gain of sediment of +64,580 m^3 on the subaerial beach (+7.5 m^3/m). The volume gained in the foreshore during the study period was +10 540 m^3 (+1.2 m^3/m), which represents 16% of the total beach volume. The remaining 84% (+54,040 m^3, +6.3 m^3/m) was accumulated on the backshore. Subaerial volume changes showed a non-homogeneous alongshore behaviour, with alternating deposition/erosion zones in the foreshore, and deposition prevailed on the backshore, particularly in the northern sector from L'Estartit to the Daro River mouth (Fig. 7). The alongshore pattern of volume changes in the foreshore is well correlated with the observed shoreline behaviour, so retreating areas showed eroding foreshore and vice versa (Fig. 6B, 7C). However, the comparison between volume changes in the subaerial part of the beach and observed shoreline changes reveals no significant relationship (Fig. 8) because retreating areas can show an increase in the overall beach volume. The only area where both variables showed a 'coherent' behaviour (shoreline advance was accompanied by volume increase and vice versa) was the southern sector of the beach, south of the Daro River mouth (Figs. 6B, 7B, 8). This different behaviour between shoreline displacements and total volume changes can be explained by the observed sediment accumulation on the backshore (Figs. 7D, 7E).

The net accumulation on the backshore comprises backshore aggradation and changes in the dune system, including dune erosion, burial of small dunes, accumulation on the interdunes and overwash deposits. Dune geomorphic changes also displayed a high alongshore variability that can be explained by alongshore variations in the beach and dune elevations that control the beach inundation potential during storms (Fig. 9). Beach and dune elevation show an increasing trend southwards, from 4.5 m in the north to 7 m in the south (Fig. 9B). From L'Estartit to the Daro River mouth, large morphological changes were observed at elevations of up to 4.5 m with respect to mean sea level and up to a distance of 135 m from the shoreline (Figs. 7E, 9). In this sector of the beach, maximum water levels during the extreme storm of December 2008 significantly exceeded the dune or berm crest. As a result, the beach was overtopped and the sand was transported landwards and deposited as overwash fans that extend tens of metres

366 landward of the dune crest (up to 80-100 m; Fig. 7E). During moderate storms, maximum water
367 levels were higher than the elevation of the base of the dune but lower than the dune crest
368 elevation, likely forcing dune erosion (Fig. 9). On the southern part of the beach, however, most
369 of the observed volume changes occurred on the foreshore, with only minor changes on the
370 backshore. This is probably due to the fact that dune and beach elevations are higher and,
371 consequently, overtopping conditions during the extreme storm were not likely to occur and
372 most of the changes were restricted to the external part of the dune system (Figs. 7E, 9).

373 To assess the influence of urbanization on the morphological response of Pals beach, areas with
374 different levels of urbanization were compared with natural areas. Urbanized areas include
375 L'Estartit, Els Griells, El Mas Pinell and Pals beach golf course, where the beach width is
376 reduced by urban construction in the hinterland (Fig. 1). The natural areas include
377 environmental protected areas within the Medes Islands and Baix Ter Natural Park and the
378 Partial Nature Reserve of the Baix Ter and Daro (Fig. 1). The morphological evolution of the
379 beach during the study period revealed a net shoreline retreat of -3.9 m and a gain of volume of
380 +9.2 m^3/m in natural areas. In urbanized areas, the beach exhibited a shoreline retreat of -4.4 m
381 and a net gain of volume of +4.7 m^3/m.

382 4.2.2 Illa Roja and Sa Riera

383 The two small embayed beaches located at the south of the study area (Illa Roja and Sa Riera)
384 behaved differently in terms of shoreline change (Fig. 10). Shoreline variations at Illa Roja
385 showed an advance in the southern sector (up to 7 m) and a retreat in the northern sector (up to
386 17 m), with a mean shoreline retreat of -3.7 ± 6.9 m and a reduction in the subaerial beach area
387 of -677 m^2 (Fig. 10C). Conversely, shoreline and emerged beach area at Sa Riera remained
388 almost constant during the study period; shoreline displacements ranged between -2.3 and +3.8
389 m, with a mean value of -0.2 ± 1.3 m and a negligible loss (-44 m^2) of the beach area (Fig. 10F).
390 At Illa Roja, the change in the orientation of the shoreline implied a decrease in the total beach
391 area but without significant volume changes (+0.4 m^3/m); sediment eroded from the northern
392 side of the beach was transported towards the south (Fig. 10C). In contrast, Sa Riera showed the

393 highest accumulation values of the three beaches, with a net gain of volume of +11.2 m^3/m,
394 mostly accumulated on the backshore (Fig. 10F).

395 **5. Discussion**

396 **5.1 Shoreline changes as a proxy for subaerial beach volume?**

397 In most morphological studies in micro-tidal environments, a usual hypothesis is that shoreline
398 variation is a good proxy of subaerial volume, which implies the existence of a strong
399 correlation between the two parameters (e.g. Lee et al., 1995; Dail et al., 2000; Sallenger et al.,
400 2002; Dingler and Reiss, 2002; Farris and List, 2007). However, the general validity of this
401 hypothesis is questioned by observed differences in the magnitude and, most important, the sign
402 of shoreline and volume changes along Pals beach. This beach shows a poor correlation (r^2 ~
403 0.43) between shoreline changes and emerged beach volume due to the observed sediment
404 accumulation on the backshore (Fig. 8A). The only part where shoreline and volume changes
405 are well correlated (r^2 ~ 0.71; Fig. 8B) is the southern sector of the beach, where most of the
406 changes were restricted to the foreshore: shoreline advances coincided with sediment deposition
407 and shoreline retreat with erosion. This finding suggests that low-lying coasts subjected to storm
408 impacts driving significant overwash processes are not a suitable environment for assuming that
409 shoreline changes properly reflect beach volume changes. The use of shoreline changes as a
410 proxy of volume changes implicitly assumes that the shape of the beach profile does not change
411 significantly over time; the entire profile migrates in the same direction as the shoreline (e.g.
412 Hanson, 1989; Dail et al, 2000; Farris and List, 2007). However, changes in the shape of beach
413 profiles such as those due to overwash processes can significantly limit the validity of this
414 proxy, in particular at short timescales. This is in agreement with other studies that observed
415 decreasing accuracies in the beach volume estimation on beaches with along- or cross-shore
416 variations in the magnitude of volume changes (Robertson et al., 2007; Theuerkauf and
417 Rodriguez, 2014).

418 The only part of the beach that shows a relative consistency between volume changes and
419 shoreline displacements is the foreshore. Along Pals beach, a good correlation (r^2 ~ 0.75) is
420 observed between measured shoreline displacements and foreshore volume changes (Fig. 8C),
421 particularly in the southern sector (r^2~0.84; Fig. 8D). In spite of this good correlation, the beach
422 experienced an overall mean shoreline retreat (-3.9 m) but a positive volume change in the
423 foreshore (+1.2 m^3/m), which should indicate that expected volume losses in the foreshore for
424 retreating parts were lower than expected when compared with sediment deposition in
425 prograding areas. The difference in magnitude and sign of the shoreline and foreshore volume
426 changes is probably related to differences in the slope and elevation of the accreting and eroding
427 sectors of the beach. Small changes in the shoreline position imply small changes in the
428 foreshore volume in low (1-1.5 m high) and gentle (β_f ~0.6) beach profiles, as observed in the
429 northern and central areas of the beach (Fig. 3A). Conversely, larger changes in the foreshore
430 volume are associated with smaller changes in the shoreline in higher (up to 3.5 m) and steeper
431 (β_f ~1.1) beach profiles, as observed in the southern sector of the beach (Fig. 3B).

432 The morphological evolution of Pals beach during the study period revealed a significant
433 increase in the emerged beach volume of +7.5 m^3/m, mostly due to large accumulation of sand
434 on the backshore (+6.3 m^3/m). This large accumulation was related to the impact of storms
435 when storm surge and waves produced overwash that deposited sand on the dune system or
436 even inland, forming overwash fans (Fig. 11) and increasing volume on the backshore. High
437 water levels associated with moderate storms also contributed to backshore aggradation through
438 overtopping of the beach berm, particularly in the northern sector where the beach topography is
439 lower and gentler (Fig. 9). During calm weather waves, swash is confined to the foreshore of the
440 beach seaward of the dune and berm crest; consequently, the sand accumulated on the
441 backshore during storms remains as a buffer deposit, resulting in larger and more permanent
442 changes on the backshore and increasing differences between shoreline and beach volume
443 change rates. The increasing volume on the backshore during energetic storms was also
444 observed on other low-lying sandy coasts (Sallenger, 2000; Doughty et al., 2006; Stockdon et

al., 2007; Gervais et al., 2012; Clemmensen et al., 2016). Stockdon et al. (2007) found that the magnitude of the beach volume change was significantly greater during energetic storms than during moderate storms due to the landward transport of sand. Similarly, in the nearby Gulf of Lions, Gervais et al. (2012) reported deposition on the backshore when the highest water levels raise the elevation of the top of the berm, and cause breaching and/or overwash of the dune system accompanied by large sand accumulation (about 8 m^3/m).

In addition to large accumulation on the backshore, Pals beach also experienced large gains of sediment on the foreshore (+1.2 m^3/m), with the largest accretion at the southernmost limit (Fig. 7C). Geomorphic changes in Pals beach suggest that the increase in foreshore volume is produced by post-storm beach recovery, alongshore sediment redistribution and fluvial sedimentary inputs. After storms, onshore reworking of storm deposits in the submerged profile usually result in onshore bar migration, followed by bar welding and foreshore accretion (Wright and Short, 1984; Morton et al., 1994; Masselink et al., 2006). On Pals beach, the post-storm beach aggradation through slip-face ridges merging to the beach is confirmed by the foreshore configuration, which is characterized by the presence of bar type morphologies attached to the shoreline with a landward–facing slip-face. The large foreshore accretion at the southernmost limit of the beach likely results from the prevailing alongshore sediment transport towards the southwest, as is also evidenced by changes in the beach planform, the southwards migration of cuspate morphologies along the shoreline, and the huge gain in sediment of Sa Riera beach (+ 11.2 m^3/m). The sand eroded from the northern Pals and Illa Roja beaches during storms is transported downdrift to Sa Riera, contributing to the recovery and infilling of the beach during post-storm conditions (Fig. 10). Finally, rivers may also locally contribute to the observed positive volume changes in the subaerial beach, particularly at the river mouth (Figs. 7, 11). Though it is very difficult to differentiate river contribution from alongshore sediment transport processes at the river mouths, the observed morphological changes and the net volume gain at the Ter and Daro River mouths (+800 m^3 and +980 m^3, respectively) suggest that rivers

471 could also be contributing to increased beach volume during short-lived flood events such as
472 that observed during the extreme storm of December 2008 (Fig. 2).

473 **5.2 Observed and predicted beach inundation**

474 The morphological evolution of Pals beach indicates the occurrence of inundation during the
475 study period, which must have occurred during the impact of the largest storm. Large sediment
476 accumulation on the backshore, and dune morphological changes, were observed in those areas
477 where maximum storm-induced water levels exceed the maximum beach and dune elevation
478 (Figs. 9, 12). The maximum distance of inundation has been defined as the landward limit of
479 overwash deposits. It was determined from observed elevation changes across the beach and
480 was measured using the initial (pre-storm) shoreline position as a reference (Fig. 12A).
481 Following the observed alongshore pattern in beach changes, the inundation distance was
482 significantly larger (up to 135 m) in the northern sector of the beach, where the beach and dunes
483 are lower and overwash deposits extend up to 80-100 m inland from the dune ridge, than in the
484 southern sector (~ 65 m), where higher dunes prevented overwash (Fig. 12B). In addition,
485 inundation distance was also strongly reduced in areas where houses and promenades occupy
486 the backshore, limiting the potential overwash transport, as observed at Els Griells.

487 The observed inundation derived from morphological changes was compared with expected
488 storm impacts based on the use of predictive models to evaluate their accuracy. The Sallenger
489 (2000) model was applied to the pre-storm beach morphology considering the maximum storm-
490 induced water levels associated to an energetic storm, the extreme storm, with a return period of
491 approx. 50 years. The distribution of the observed inundation along Pals beach is consistent
492 with the predicted regime based on the storm impact scaling model proposed by Sallenger
493 (2000). Larger inundation distances and larger changes in the dune system were observed on the
494 northern part of the beach, where beach and dune morphologies and the total water level
495 determined the prevalence of the overwash and inundation regimes during the impact of the
496 extreme storm of December 2008 (Fig. 12). On the other hand, dune changes were almost
497 negligible and a shorter inundation distance was observed in the southern sector, where the

conditions determined the existence of the collision regime during that storm. These findings should indicate the validity of this conceptual model for predicting the response of low-lying coasts to storm impacts.

The observed inundation was compared with existing assessments of regional vulnerability to storm impacts (Mendoza, 2008; Bosom, 2014). The first aspect to be considered is that these methods were developed to be applied at a regional scale and therefore represent the beach morphology along the beach in a simplified manner by just using two profiles for the northern and southern parts. Also, they are not applied to a specific storm, such as the one analysed in this work, but to characteristic storm conditions obtained from cluster analysis (Mendoza, 2008) or from extreme probabilistic distributions (Bosom and Jiménez, 2011; Bosom, 2014). Therefore, these methods only indicate the expected overall behaviour of the beach in response to storm impacts without reproducing the observed alongshore small-scale variability. Nevertheless, these general vulnerability assessment methods indicate that the northern part of the beach has a much greater vulnerability to inundation during storms than the southern part, which showed a very low vulnerability (Fig. 12). As shown in Fig. 12C, the length of the inundated area during the peak of the extreme storm represented 75%, 77%, 60% and 37% of beach length based on our observations, and on expected overwash and inundation regimes following the models of Sallenger (2000), Mendoza (2008) and Bosom (2014), respectively. In addition to the total length differences, many locations defined in the predictions as areas with low vulnerability to inundation were overwashed during the extreme storm (Fig. 12). Discrepancies between the observed inundation and expected storm impact are mainly due to differences in the prediction associated with measurements of beach morphology and estimates of storm-induced water levels during the specific storm. The accuracy of predicted vulnerability to inundation strongly depends on the quality of beach morphological parameters that vary significantly alongshore, such as beach and dune elevation and foreshore slope, beach width or dune volume. Therefore, good quality topographic data are necessary to properly define the

524 spatial variations in the beach susceptibility to inundation during storms, particularly for
525 beaches with high alongshore variability.

526 Furthermore, the beach morphology varies with time, affecting the differences between the
527 observed and expected storm impact. The variations can be clearly observed in Table 4, where
528 predicted storm impact using two different datasets for the same beach (pre-storm and post-
529 storm LiDAR-derived topographies) and the same storm are shown. The predicted overwash
530 and inundation regimes during the extreme storm of December 2008 varies between 77% and
531 64% of the total beach length for pre-storm and post-storm beach morphologies, respectively. It
532 is also interesting to note that the predicted overwash and inundation regimes are reduced in
533 2009 (after the impact of the extreme storm) in comparison with the pre-storm morphology
534 (2008), probably due to higher beach elevations produced by large accumulation on the
535 backshore. These observations highlight the need to regularly update the morphological
536 indicators used for predicting beach vulnerability in order to represent the pre-storm beach
537 conditions.

538 **5.3 Influence of urbanization on the beach response**

539 Existing studies of storm-induced changes in low-lying coasts reported different behaviour
540 between natural and urban areas related to the decrease in the beach width caused by urban
541 development in the hinterland (Morton et al., 1994; Saye et al., 2005; Gervais et al., 2012;
542 Jiménez et al., 2012; Richter et al., 2013, among others). Morton et al. (1994) observed that
543 beach recovery is prevented in urbanized areas because the beach seaward of houses, roads and
544 promenades is too narrow to permit an efficient cross-shore sediment transport and dune
545 construction. Gervais et al. (2012) reported an increase in coastal vulnerability to extreme
546 storms of urbanized areas along the Gulf of Lion coastline in relation to natural coastal barriers.
547 Overwash and/or breaching of the dune system dominate in natural areas, whereas severe
548 damage to coastal infrastructures and facilities is observed in urbanized ones. Jiménez et al.
549 (2012) also observed that anthropogenic intervention along the Catalan coast causes significant
550 changes in beach response, intensifying erosion and inundation during storms.

The influence of urbanization on the morphological response of Pals beach is evidenced by comparing the morphological response of areas with different levels of urbanization and natural areas (Figs. 13A, 13B). The morphological evolution of the beach during the study period revealed a similar net shoreline retreat in both pristine and urbanized areas. However, the volume change, particularly accumulation on the backshore, on natural areas was two times higher than at locations where the beach had been artificially narrowed. The smaller accumulation of sediment in urban areas can be explained by the blocking effect of infrastructure, which prevents the landward transport and accumulation of sediment during storms (Fig. 13A). On the other hand, natural areas showed a significant increase in sediment volume on the backshore as a result of storm-induced overwash transport. However, though the anthropogenic influence is more subtle in these areas, the results also revealed alongshore variations in the morphological beach response related to small human interventions. These variations were observed in the dune system northwards of the Ter River mouth, where the sand was transported landwards through artificial cuts between dunes, such as beach access roads and walking paths (Fig. 11).

Identifying coastal areas at risk of flooding, determining the flood extent and assessing the human influence on the beach response are particularly important in Pals Bay due to its high natural value. A large extent of the littoral plain is protected by the Plan for Areas of Natural Interest (*Pla d'Espais d'Interès Natural*, PEIN) of Catalonia and the Natura 2000 network of the European Union. The management of Natura 2000 sites includes interests for coastal protection and users, since human activities are not excluded in these areas. It is fully recognized that humans are an integral part of nature, so human activities must be regulated in these areas, giving priority to increasing coastal resilience and maintaining a healthy sediment balance in the coastal system. Taking into account the inundation observed along Pals beach and the more resilient beach response to storms in natural areas, a minimum distance of between 65 and 135 m should be applied in the definition of the setback line. This distance corresponds to the maximum observed inundation and will serve to promote coastal resilience in this area by

enhancing sediment deposition in the hinterland. Strictly speaking, this setback should be effective for storms similar to the recorded one, which had an associated return period of approx. 50 years. Moreover, as has been demonstrated in this analysis, the extension and magnitude of the deposition are modulated by beach morphology, so the aforementioned distance will also be controlled by the dune/beach morphology. As a general rule, the lower the dune is, the larger the distance will be. Finally, it should also be considered that, in a context of climate change with sea-level rise and induced background erosion; longer setback distances for 'no development zones' should be required to reduce coastal vulnerability to storm impacts.

6. Conclusions

The morphological evolution of a low-lying embayed beach bounded by a dune system in the NW Mediterranean coast was quantified using LiDAR derived high-resolution topographic data collected prior to, and six months after, the impact of an 'extreme' storm with a return period of approx. 50 years. Results revealed a net shoreline retreat and, consequently, a loss of the emerged area, but a significant sediment gain on the subaerial beach. The opposite behaviour between shoreline and subaerial beach volume changes is related to storm impacts driving significant overwash processes that transport sediment landwards and increasing volume on the backshore.

The use of repeated high-resolution topographic data to quantify beach geomorphic changes has proven to be a valuable tool for estimating subaerial beach volume changes in relation to other proxies such as changes in beach profiles and shoreline positions. Results from this study indicate that shoreline displacements may not properly represent beach volume changes on low-lying coasts, where overwash processes during storms are significant due to the cross-shore redistribution of beach sediment. Observations also suggest that beach transects may not resolve volume for beaches with variable morphology alongshore at short time scales (months). Accordingly, closely spaced beach profiles or segmentation of the beach into bins should be necessary to capture along-shore volume changes associated to beach complexities such as those resulting from beach cusps or dunes.

605 Observed morphological changes evidenced the impact of the storm and the subsequent beach
606 recovery and revealed significant spatial variability in the beach response. The impact of the
607 extreme storm on the beach morphology is evidenced by large accumulation on the backshore
608 and the formation of overwash deposits. On the other hand, the net gain of sediment on the
609 foreshore and the formation of second-order morphologies along the shoreline evidence beach
610 recovery after the storm. This alongshore variability of the morphological response is strongly
611 related to alongshore variations in the beach morphology, such as smaller-scale morphologies
612 along the shoreline, beach and dune elevations and foreshore slope. Changes in the morphology
613 (amplitude and/or extension) and migration of megacusps over the study period produce a
614 differential erosion/accretion pattern along the beach that results in a high variability in the
615 shoreline position. On the other hand, the magnitude and alongshore variability of
616 morphological changes on the backshore are related to the impact of the extreme storm and are
617 modulated by beach morphology, and particularly the dune/beach elevation and the beach slope.
618 Larger geomorphic changes are observed where beach dunes are lower, favouring the
619 dominance of overwash conditions, whereas beach changes are limited to the foreshore where
620 beach dunes are higher.

621 The comparison between observed and expected storm inundation highlights the need to obtain
622 high-quality, updated coastal topographic data to properly define the spatial variations in beach
623 inundation during storms. Observed inundation is in agreement with the model of Sallenger
624 (2000) using pre-storm beach topography, but it is slightly different from the storm regime
625 expected from post-storm beach topography because of temporal changes in the beach
626 morphology. Similarly, the observed inundation also differs from existing regional assessments
627 of vulnerability to storm impacts, as these methods focus on the expected overall behaviour of
628 the beach in response to storm impacts without reproducing the observed alongshore small-scale
629 variability.

630 Finally, alongshore variability in the beach response can be also modulated to anthropogenic
631 intervention on the backshore or the foredune. The comparison between natural and urban areas

evidences a better post-storm beach recovery of natural beaches, although the latter also reveal the influence on the beach response of small anthropogenic interventions such as regulated pathways and walking paths. Based on the alongshore variability of the beach inundation during storms and the increasing resilience of natural areas, a minimum distance corresponding to the maximum observed inundation should be assumed in the definition of the setback line in low-lying coasts in order to increase coastal resilience.

Acknowledgements

This study was conducted within a collaboration agreement between the Institute of Marine Sciences (ICM-CSIC) and the Institut Cartogràfic i Geològic de Catalunya (ICGC), with the aim of analysing the usefulness of LiDAR data for monitoring coastal processes. It was supported by the FORMED (CGL2012-33989) Project funded by the Spanish Ministry of Economy and Competitiveness. R. Durán is supported by a CSIC JAE-Doc contract co-funded by the FSE. JAJ was funded by the RISC-KIT (Grant No 603458) and PaiRisC-M (CTM2011-29808) projects funded by the European Union and the Spanish Ministry of Economy and Competitiveness, respectively. The authors would also like to thank Josep Pascual for providing water level data from L'Estartit tidal gauge.

References

ACA (Agència Catalana de l'Aigua), 2002. Estudi d'actualització de l'avaluació de recursos hídrics a les conques internes de Catalunya. Generalitat de Catalunya, Departament de Medi Ambient, Barcelona, Spain.

Bolaños, R., Jorda, G., Cateura, J., Lopez, J., Puigdefabregas, J., Gomez, J., Espino, M., 2009. The XIOM: 20 years of a regional coastal observatory in the Spanish Catalan coast. J. Mar. Syst. 77, 237–260.

655 Bosom, E., Jiménez, J.A., 2011. Probabilistic coastal vulnerability assessment to storms at
656 regional scale – application to Catalan beaches (NW Mediterranean). Nat. Hazards Earth
657 Syst. Sci. 11, 475–484.

658 Bosom, E. 2014. Coastal vulnerability to storms at different time scales. Application to the
659 Catalan coast. Ph.D. Thesis, Universitat Politècnica de Catalunya, Spain.

660 CIIRC, 2010. Estat de la Zona Costanera a Catalunya. Departament Política Territorial i Obres
661 Públiques, Barcelona.

662 Clemmensen, L.B., Glad, A.C., Kroon, A., 2016. Storm flood impacts along the shores of
663 micro-tidal inland seas: A morphological and sedimentological study of the Vesterlyng
664 beach, the Belt Sea, Denmark. Geomorphology 253, 251–261.

665 Cros, L., Serra, J., 1993. A complex dune system in Baix Empordà (Catalonia, Spain). Geol.
666 Soc., London, SP, 72, 191–199.

667 Dail, H.J., Merrifield, M.A., Bevis, M., 2000. Steep beach morphology changes due to energetic
668 wave forcing. Mar. Geol. 162, 443–458.

669 de Vries, S., Southgate, H.N., Kanning, W., Ranasinghe, R., 2012. Dune behavior and aeolian
670 transport on decadal timescales. Coast. Eng. 67, 41–53.

671 Dingler, J.R., Reiss, T.E., 2002. Changes to Monterey Bay beaches from the end of the 1982–83
672 El Niño through the 1997–98 El Niño. Mar. Geol. 181, 249–263.

673 Directive 2007/60/EC of the European Parliament and of the Council of 23 October 2007 on the
674 Assessment and Management of Flood Risks, 2007.

675 Doughty, S.D., Cleary, W.J., McGinnis, B. A., 2006. The recent evolution of storm-influenced
676 retrograding barriers in southeastern North Carolina, USA. J. Coast. Res. 1, 122–126.

677 Farris, A.S., List, J.H., 2007. Shoreline Change as a Proxy for Subaerial Beach Volume Change.
678 J. Coast. Res. 233, 740–748.

679 Fiore, M.M.E., D'Onofrio, E.E., Pousa, J.L., Schnack, E.J., Bértola, G.R., 2009. Storm surges
680 and coastal impacts at Mar del Plata, Argentina. Cont. Shelf Res. 29, 1643–1649.

681 Font, J., 1990. A comparison of seasonal winds with currents on the continental slope of the
682 Catalan Sea (northwestern Mediterranean). J. Geophys. Res. Ocean. 95, 1537–1545.

683 Gervais, M., Balouin, Y., Belon, R., 2012. Morphological response and coastal dynamics
684 associated with major storm events along the Gulf of Lions Coastline, France.
685 Geomorphology 143-144, 69–80.

686 Grau, J., Bosch, E., Talaya, J., 2012. La transición de la geoinformación oficial a ETRS89 en
687 Catalunya. Rev. Catalana de Geografía, IV Època XVII, 45.

688 Hanson H. 1989. GENESIS: a generalized shoreline change numerical model. J. Coast. Res. 5,
689 1–27.

690 Houser, C., Hapke, C., Hamilton, S., 2008. Controls on coastal dune morphology, shoreline
691 erosion and barrier island response to extreme storms. Geomorphology 100, 223–240.

692 Houser, C., Wernette, P., Rentschlar, E., Jones, H., Hammond, B., Trimble, S., 2015. Post-storm
693 beach and dune recovery: Implications for barrier island resilience. Geomorphology 234, 54–
694 63.

695 Jiménez, J. A., Sancho-García, A., Bosom, E., Valdemoro, H.I., Guillén, J., 2012. Storm-
696 induced damages along the Catalan coast (NW Mediterranean) during the period 1958–2008.
697 Geomorphology 143-144, 24–33.

698 Keijpers, J.G.S., Poortinga, A., Riksen, M.J.P.M., Maroulis, J., 2014. Spatio-temporal
699 variability in accretion and erosion of coastal foredunes in the Netherlands: regional climate
700 and local topography. PLoS One 9, e91115.

701 Kornus, W., Ruiz, A., 2003. Strip Adjustment of LIDAR data. International Archives of
702 Photogrammetry and Remote Sensing 34, part 3/W13, pp. 47–50.

703 Lee, G., Nicholls, R.J., Birkemeier, W.A., Leatherman, S.P., 1995. A Conceptual Fairweather-
704 Storm Model of Beach Nearshore Profile Evolution at Duck, North Carolina, U.S.A. J.
705 Coast. Res. 11, 1157–1166.

706 Liquete, C., Canals, M., Ludwig, W., Arnau, P., 2009. Sediment discharge of the rivers of
707 Catalonia, NE Spain, and the influence of human impacts. J. Hydrol. 366, 76–88.

708 Marquès, M.A., Julià R., 2005. Evolución de la zona litoral del Empordà durante el último
709 milenio. In: Sanjaume, E., Mateu. E. (Eds.), Geomorfología Litoral i Quaternari. Universitat
710 de Valencia, Spain, pp. 259–272.

711 Marquès, M.A., Julià R., Montaner, J. 2011. Las dunas de la costa norte catalana. In: Sanjaume,
712 E., García F.J. (Eds.), Las dunas en España. Sociedad Española de Geomorfología, pp. 187-
713 204.

714 Masselink, G., Kroon, A., Davidson-Arnott, R.G.D., 2006. Morphodynamics of intertidal bars
715 in wave-dominated coastal settings — A review. Geomorphology 73, 33–49.

716 Mendoza, E.T., 2008. Coastal Vulnerability to storms in the Catalan Coast. Ph.D. Thesis,
717 Universitat Politècnica de Catalunya, Spain.

718 Mendoza, E T, Jiménez, J.J.A., 2009. Regional vulnerability analysis of Catalan beaches to
719 storms. Proc. Inst. Civ. Eng. Marit. Eng. 162, 127–135.

720 Mendoza, E.T., Jiménez, J. J.A., Mateo, J., 2011. A coastal storms intensity scale for the
721 Catalan sea (NW Mediterranean). Nat. Hazards Earth Syst. Sci. 11, 2453–2462.

722 Montaner Roviras, J., Solà Subiranas, J., 2004. Reconstrucció d'estadis paleogeogràfics recents
723 a la plana del Baix Ter. Papers de Montgri 23, 8e26.

724 Montaner, J., Julià, R., Marquès, M.A., Solà, J., Pons, P., López, J., 2010. Canvis en la
725 paleomorfologia i dinámica fluvial del riu Ter des dels darrer màxim glacial. Estudis del
726 Baix Empordà 29, 9–21.

727 Moreno, L. J., Kraus, N. C., 1999. Equilibrium shape of headland-bay beaches for engineering
728 design. Proc. Int. Cong. Coastal Sediments'99, Long Island, NY, pp. 860–875.

729 Morton, R.A., Paine, J.G., Gibeaut, J.C., 1994. Stages and Durations of Post-Storm Beach
730 Recovery, Southeastern Texas Coast, U.S.A. J. Coast. Res. 10, 884–908.

731 Morton, R.A., 2002. Factors Controlling Storm Impacts on Coastal Barriers and Beaches: A
732 Preliminary Basis for near Real-Time Forecasting. J. Coast. Res. 18, 486–501.

733 Muñoz-Perez, J.J., Payo, A., Roman-Sierra, J., Navarro, M., Moreno, L., 2012. Optimization of
734 beach profile spacing: an applicable tool for coastal monitoring. Sci. Mar. 76, 791–798.

735 Nicholls, R.J., Hanson, S.E., Lowe, J.A., Warrick, R.A., Lu, X., Long, A.J., 2014. Sea-level
736 scenarios for evaluating coastal impacts. Wiley Interdiscip. Rev. Clim. Chang. 5, 129–150.

737 Ojeda, E., Guillén, J., 2008. Shoreline dynamics and beach rotation of artificial embayed
738 beaches. Mar. Geol. 253, 51–62.

739 PAP/RAC, 2007. Protocol on Integrated Coastal Zone Management in the Mediterranean (as
740 signed in Madrid on 21 January 2008).

741 Pearre, N.S., Puleo, J.A., 2009. Quantifying Seasonal Shoreline Variability at Rehoboth Beach,
742 Delaware, Using Automated Imaging Techniques. J. Coast. Res. 25, 900–914.

743 Richter, A., Faust, D., Maas, H.-G., 2013. Dune cliff erosion and beach width change at the
744 northern and southern spits of Sylt detected with multi-temporal Lidar. Catena 103, 103–111.

745 Robertson, W., Zhang, K., Whitman, D., 2007. Hurricane-induced beach change derived from
746 airborne laser measurements near Panama City, Florida. Mar. Geol. 237, 191–205.

747 Sabater, S., Guasch, H., Martí, E., Armengol, J., Vila, M., Sabater, F. 1992. The Ter, a
748 Mediterranean river system in Spain. Limnetica 8, 141-149.

749 Sallenger, A.H. Jr. 2000. Storm impact scale for barrier islands. J. Coast. Res. 16, 890-895.

750 Sallenger, A.H., Krabill, W., Brock, J., Swift, R., Manizade, S., Stockdon, H., 2002. Sea-cliff
751 erosion as a function of beach changes and extreme wave runup during the 1997-1998 El
752 Niño. Mar. Geol. 187, 279–297.

753 Sallenger Jr., A.H., Krabill, W.B., Swift, R.N., Brock, J., List, J., Hansen, M., Holman, R.A.,
754 Manizade, S., Sontag, J., Meredith, A., Morgan, K., Yunkel, J.K., Frederick, E.B., Stockdon,
755 H., 2003. Evaluation of Airborne Topographic Lidar for Quantifying Beach Changes. J.
756 Coast. Res. 19, 125–133.

757 Sancho-García, A., Guillén, J., Ojeda, E., 2013. Storm-induced readjustment of an embayed
758 beach after modification by protection works. Geo-Marine Lett. 33, 159–172.

759 Saye, S.E., van der Wal, D., Pye, K., Blott, S.J., 2005. Beach–dune morphological relationships
760 and erosion/accretion: An investigation at five sites in England and Wales using LIDAR
761 data. Geomorphology 72, 128–155.

762 Stockdon, H.F., Jr., A.H.S., List, J.H., Holman, R.A., 2002. Estimation of Shoreline Position
763 and Change Using Airborne Topographic Lidar Data. J. Coast. Res. 18, 502–513.

764 Stockdon, H.F., Holman, R.A., Howd, P.A., Sallenger, A.H., 2006. Empirical parameterization
765 of setup, swash, and runup. J. Coast. Res SI 53, 573–588.

766 Stockdon, H.F., Sallenger, A.H., Holman, R.A., Howd, P.A., 2007. A simple model for the
767 spatially-variable coastal response to hurricanes. Mar. Geol. 238, 1–20.

768 Stockdon, H.F., Doran, K.S., Sallenger, A.H., 2009. Extraction of Lidar-based dune-crest
769 elevations for use in examining the vulnerability of beaches to inundation during Hurricanes.
770 J. Coast. Res. SI 53, 59–65.

771 Theuerkauf, E.J., Rodriguez, A.B., 2012. Impacts of Transect Location and Variations in Along-
772 Beach Morphology on Measuring Volume Change. J. Coast. Res. 282, 707–718.

773 Theuerkauf, E.J., Rodriguez, A.B., 2014. Evaluating proxies for estimating subaerial beach
774 volume change across increasing time scales and various morphologies. Earth Surf. Process.
775 Landforms 39, 593–604.

776 Willis, C.M., Griggs, G. 2003. Reductions in fluvial sediment discharge by coastal dams in
777 California and implications for beach sustainability. J. Geo. 111, 167–182.

778 Wright, L. Short, A., 1984. Morphodynamic variability of surf zones and beaches: A synthesis.
779 Mar. Geol. 56, 93–118.

780 Zhang, K., Douglas, B., Leatherman, S., 2002. Do storms cause long-term beach erosion along
781 the U.S. East Barrier Coast? J. Geol. 110, 493–502.

782 Zhang, K., Whitman, D., Leatherman, S., Robertson, W., 2005. Quantification of Beach
783 Changes Caused by Hurricane Floyd Along Florida's Atlantic Coast Using Airborne Laser
784 Surveys. J. Coast. Res. 21, 123–134.

785

Figure captions

Figure 1. (A) Location map of Pals Bay. (B) Shaded relief and topographic map of the Baix Empordà showing the main morphological features, such as river channels and palaeochannels and dunes (Cros and Serra, 1993; ACA, 2002; Marquès et al., 2011). (C) Orthophoto collected in 2008 including the three beaches that comprise Pals Bay: Pals, Illa Roja and Sa Riera. Location of rainfall, water river discharge and tidal gauging stations used in this study are also shown. Topographic data from the Institut Cartogràphic i Geològic de Catalunya.

Figure 2. Time series of rainfall and river flows derived from the rain gauge at Girona (A), and two river gauging stations at the Ter (B) and Daro (C). Data provided by the Agència Catalana de l'Aigua (ACA). See Figure 1 for location.

Figure 3. Two representative beach profiles in the northern (A) and southern (B) sectors of the beach showing the morphological parameters used to characterize beach changes: volume changes on the backshore and the foreshore, and changes in the shoreline position (ΔX). Variables used in scaling the impact of storms are also shown: D_{low}, D_{high}, R_{low} and R_{high}.

Figure 4. Scatter plot representing the relative beach volume with increasing distance between profiles. Ten different profile locations were evaluated for each profile spacing. The thick grey line indicates the beach volume obtained from the difference between the two DEMs.

Figure 5. Time series of (A) significant wave height (H_s), (B) peak period (T_p) and (C) water level (WL) derived from the Palamós wave buoy and the L'Estartit tidal gauge. See Figure 1 for location. (D) Maximum storm-induced water levels during the study period considering the mean foreshore slope (β_f = 0.11). Grey bars represent moderate storm events that occurred during the study period. The most energetic storm is highlighted in dark grey.

Figure 6. Shoreline variations in Pals beach during the study period: (A) Ortophoto of Pals beach collected in 2008 with the shoreline position in 2009 superimposed (black line); (B) variations in the shoreline position; (C) and (D) hyperbolic tangent fit for the initial (2008) and

811 final (2009) shoreline, respectively; (E) and (F) smaller-scale morphology of the initial and final
812 shoreline, respectively. Positive values correspond to shoreline advance, whereas negative
813 values indicate landward displacement of the shoreline position. Note the presence of large,
814 rhythmic morphologies superimposed on megacusps (grey line in Figs. 5E and 5F).

815 **Figure 7**. (A) Orthophoto of Pals beach collected in 2009. Volume changes: (B) subaerial
816 beach; (C) foreshore; (D) backshore; and (E) across- and alongshore variations in the subaerial
817 beach volume.

818 **Figure 8**. Relationship between shoreline variations and beach volume changes calculated on
819 the basis of closely spaced (1 m) beach profiles: (A) along Pals beach and (B) along the
820 southern sector of the beach, from the Daro River mouth to the southernmost end of the beach.
821 Shoreline changes and foreshore volume: (C) along Pals beach and (D) along the southern
822 sector of the beach.

823 **Figure 9.** (A) Volume changes in the dune system including overwash deposits. (B)
824 Morphological changes along the dune ridge. (C) Alongshore variation of high water levels
825 during calm conditions, moderate storms and the extreme storm superimposed on beach and
826 dune elevations.

827 **Figure 10**. Morphological changes in the small beaches during the study period: (A) initial
828 orthophoto, (B) final orthophoto and, (C) shoreline position and volume changes in Illa Roja
829 beach. (D) Initial orthophoto, (E) final orthophoto, and (F) shoreline position and volume
830 changes of Sa Riera beach.

831 **Figure 11**. Orthophotos showing the main morphological changes in the northern sector of Pals
832 beach collected in (A) May 2008 (before the storm) and (B) June 2009 (6 months after the
833 storm). (C) Beach volume changes. Black line represents the maximum observed inundation.
834 See Figure 7 for location.

Figure 12. (A) Orthophoto collected in 2008 and maximum observed inundation (black line). (B) Maximum inundation distance. (C) Predicted inundation regimes from pre-storm morphology following the model of Sallenger (2000), flood vulnerability index by Mendoza (2008) and vulnerability to storm inundation by Bosom (2014).

Figure 13. (A) Orthophoto of Pals beach at Els Griells, (B) Orthophoto of a natural area within Pals beach. See Figure 1 for location.

842 **Table captions**

843 **Table 1**. LiDAR flight parameters. Leica ALS50-II system.

844 **Table 2**. Absolute height accuracy of LiDAR data.

845 **Table 3**. Characteristics of the storms identified during the study period. Maximum storm water
846 levels were calculated for each event, considering the mean and standard deviation of the
847 foreshore slope (β_f = 0.11 ± 0.03). Storm event *i* corresponds to a double-peaked storm. The
848 most energetic event during the study period (event *v*) appears in bold.

849 **Table 4**. Occurrence of the storm impact regime predicted by applying the model of Sallenger
850 (2000) to the pre-storm (2008) and post-storm (2009) beach morphologies. Percentages in
851 relation to the total beach length.

Table

Table 1

	2008-Oct-16	2009-Aug-11,22
Scan angle (º)	56	62
Scan rate (Hz)	22	30.6
Point repetition frequency (Hz)	88000 MPiA	90600 SPiA
Above ground level (m)	2250	1000
Speed (knots)	140-165	112-136
Strip width (m)	2393	1200
Average point density (m^{-2})	0.37	1.05
Nadir point density (m^{-2})	0.25	0.72
Footprint diameter(m)	0.58	0.23
Precision in height (cm)	15	9
Precision in plan (cm)	32	14
Strips in adjustment	31	36

Table

Table 2

	2008-Oct-16	2009-Aug-11,22
N	54	54
Average dz (m)	-0.08	-0.11
RMS (m)	0.09	0.11
Sigma (m)	0.03	0.02

N: number of observations. dz: height difference. RMS: vertical root mean square.

Table

Table 3

Event	Initial data	Hs (m)	Tp (s)	Hmax (m)	Duration (h)	Mean wave direction	Rhigh (m) (β_f = 0.11 ± 0.03)
i	2008-10-31	2.8	8	4.5	68	S	1.6 ± 0.4
		3.3	8.5	5.8		S	1.9 ± 0.4
ii	2008-11-27	3.4	11.1	6	41	NE	2.5 ± 0.6
iii	2008-11-29	2.8	9.8	4.3	37	S	1.9 ± 0.5
iv	2008-12-15	2.9	8.9	4.8	17	N	1.8 ± 0.4
v	**2008-12-26**	**7.5**	**12.2**	**14.4**	**83**	**E**	**4.1 ± 1.1**
vi	2009-01-23	2.9	9.1	4.6	33	N	2.1 ± 0.4

Table

Table 4

		2008 morphology	2009 morphology
Extreme storms	Inundation	3%	2%
	Overwash	74 %	62 %
	Collision	22 %	30 %
	Swash	1 %	6 %
Moderate storms	Overwash	10 %	7 %
	Collision	16 %	5 %
	Swash	74 %	88 %

Figure (Color)

Click here to download high resolution image

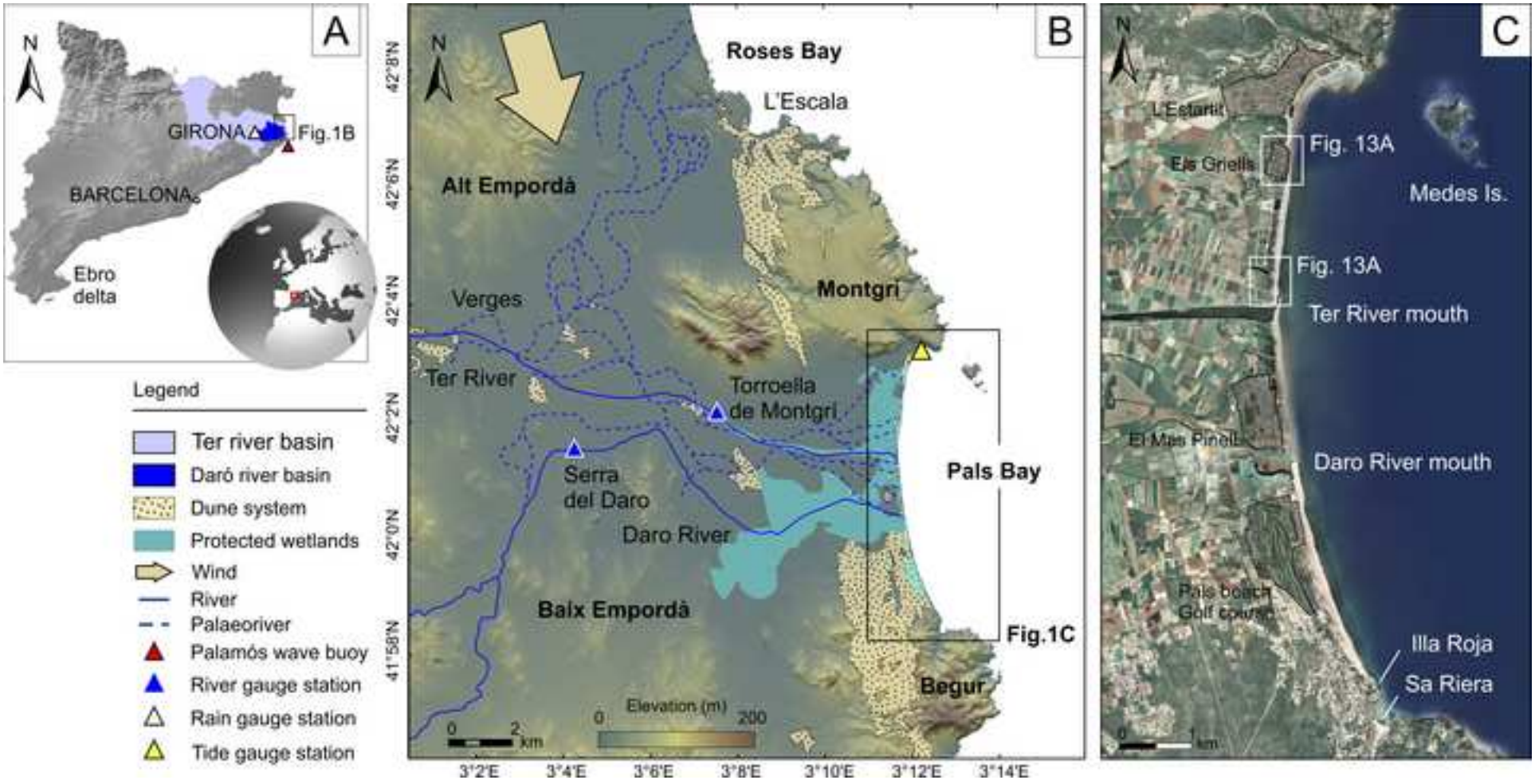

Figure (Color)
Click here to download high resolution image

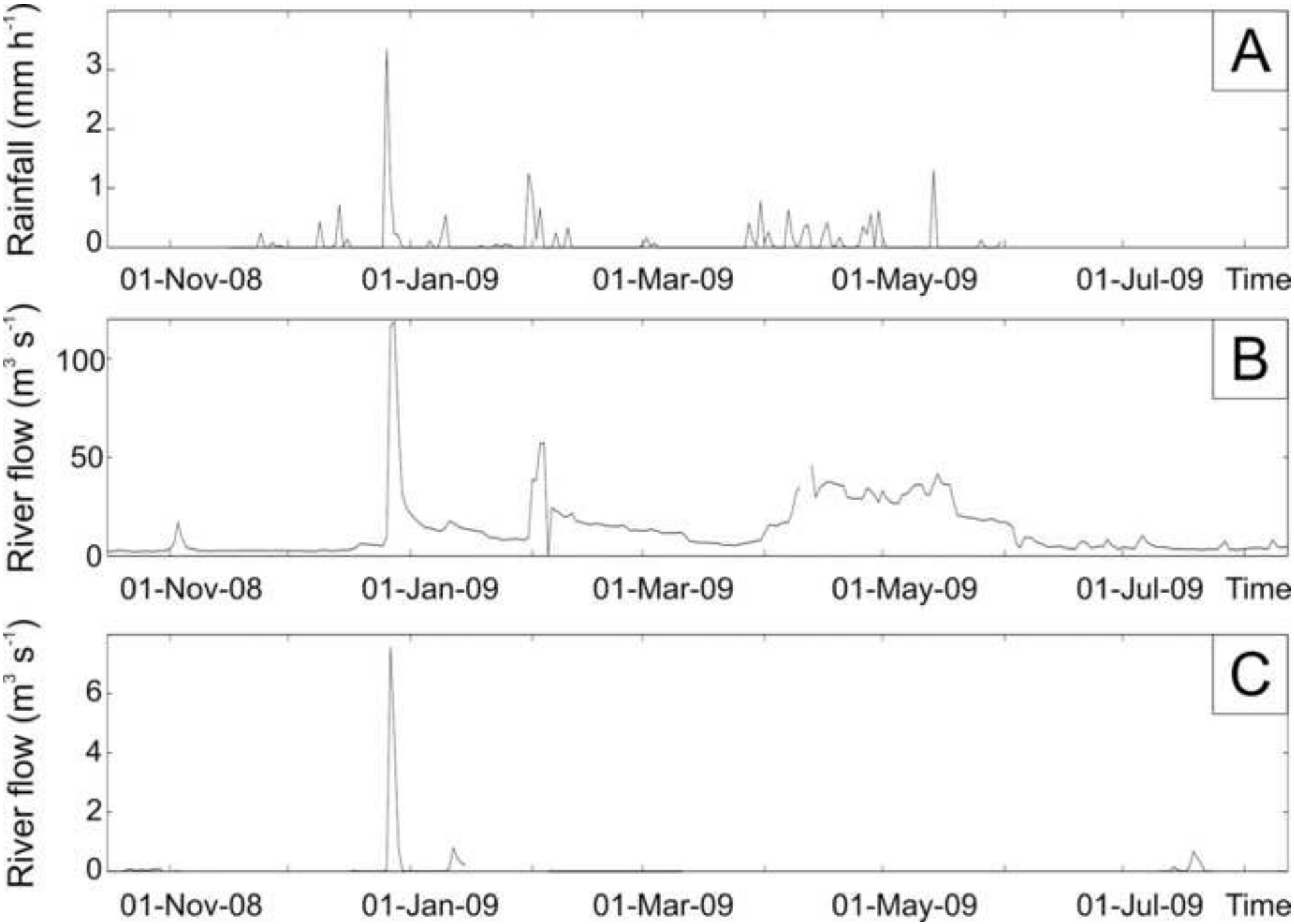

Figure (Color)

Click here to download high resolution image

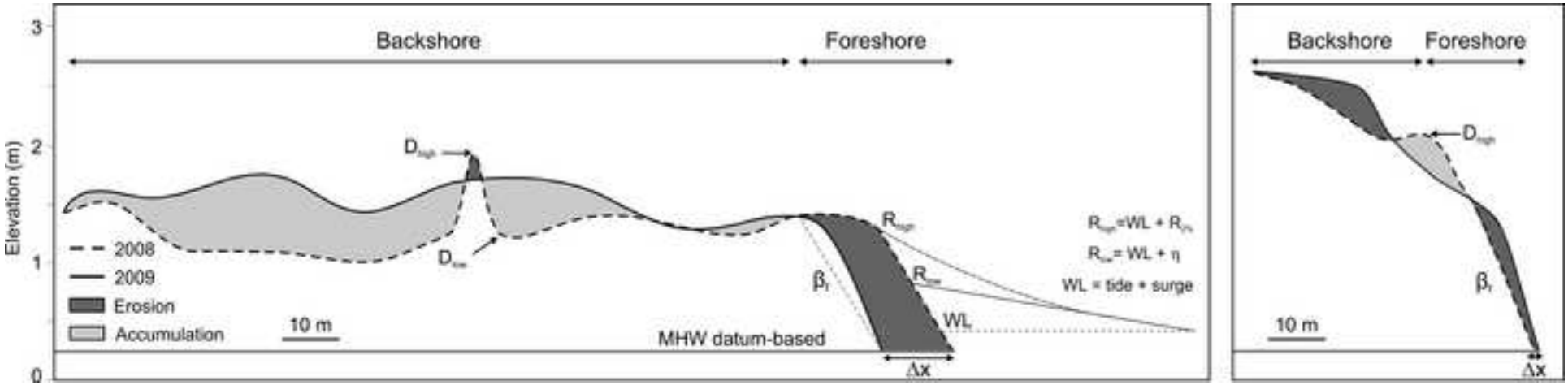

Figure (Color)
Click here to download high resolution image

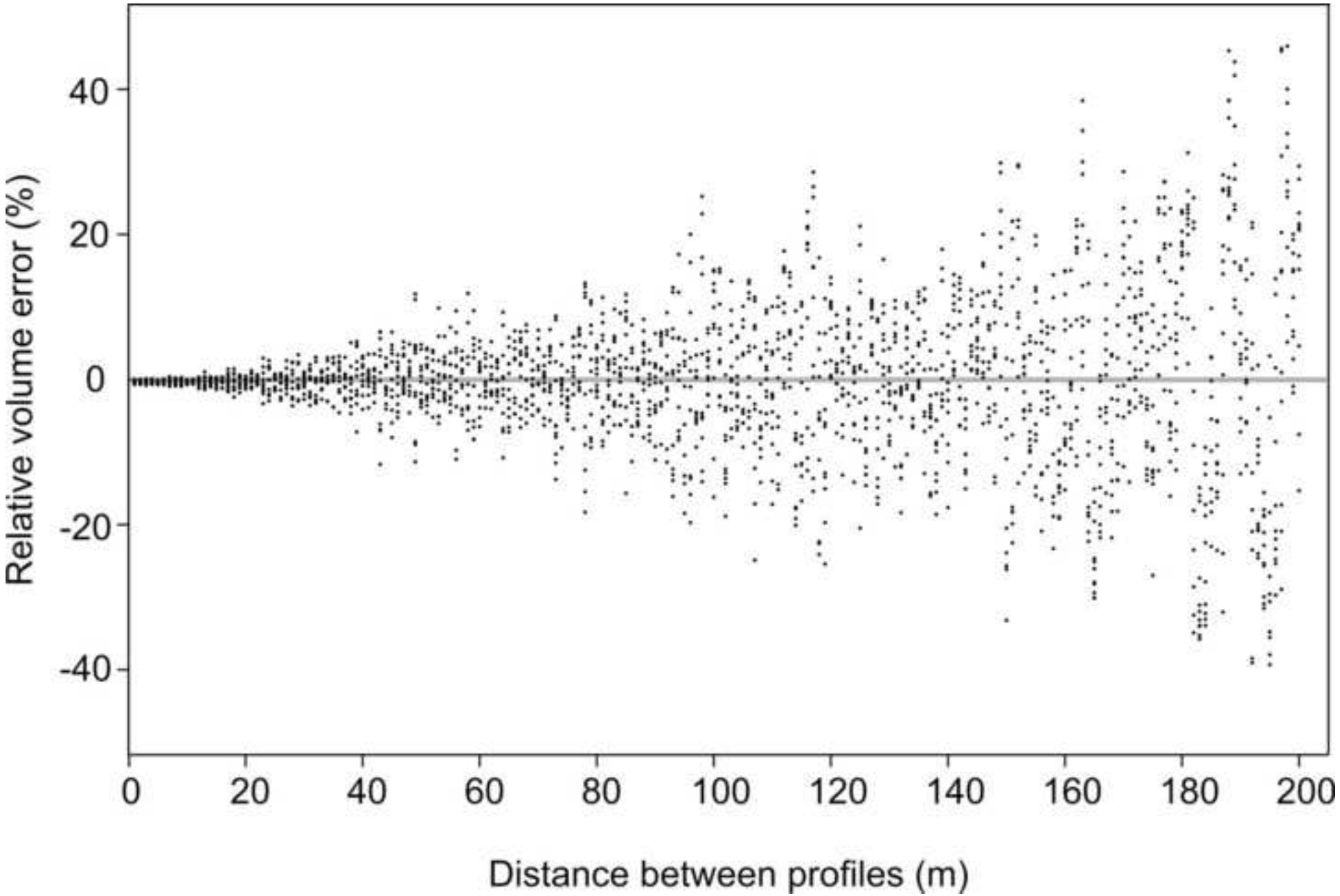

Figure (Color)

Click here to download high resolution image

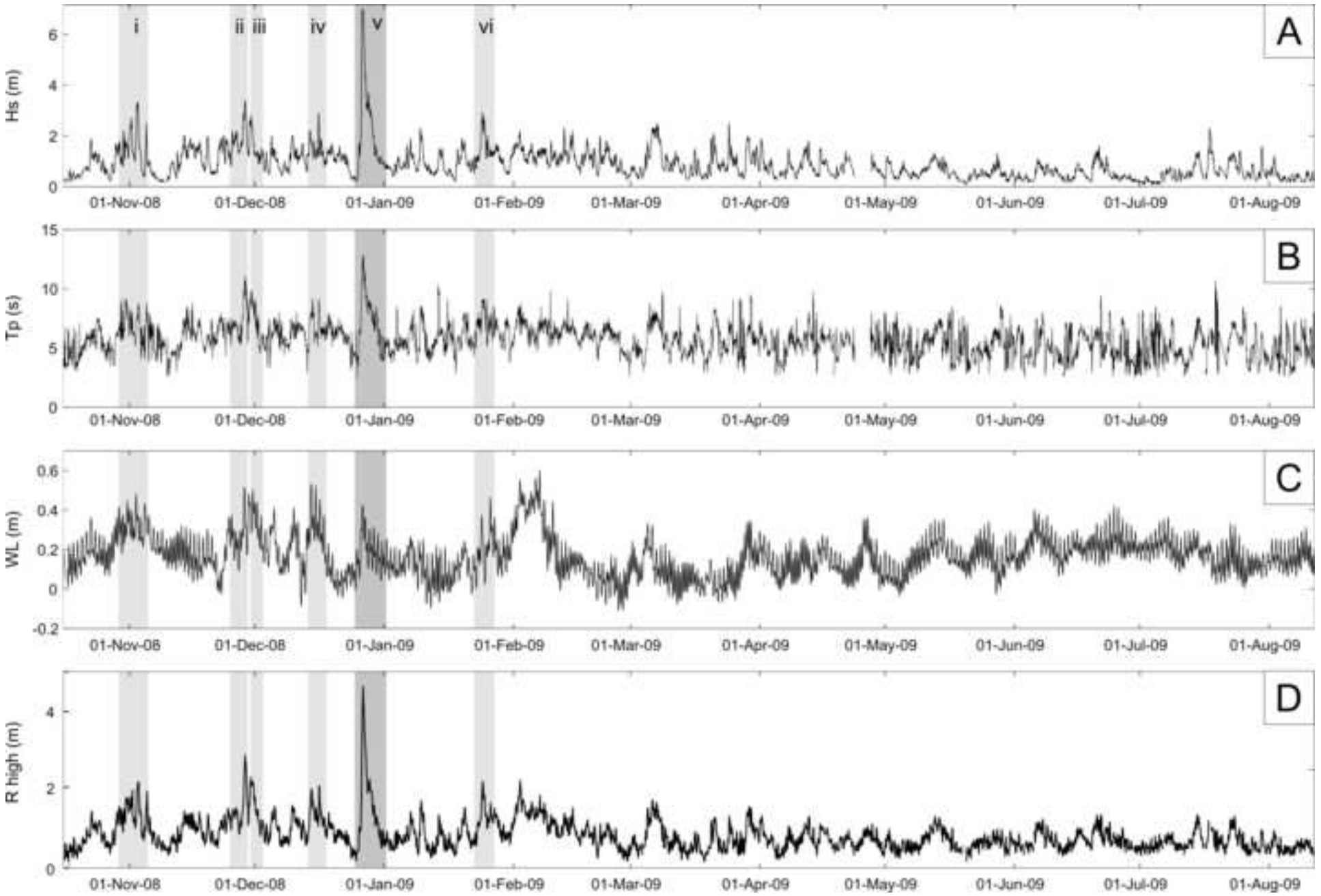

Figure (Color)

Click here to download high resolution image

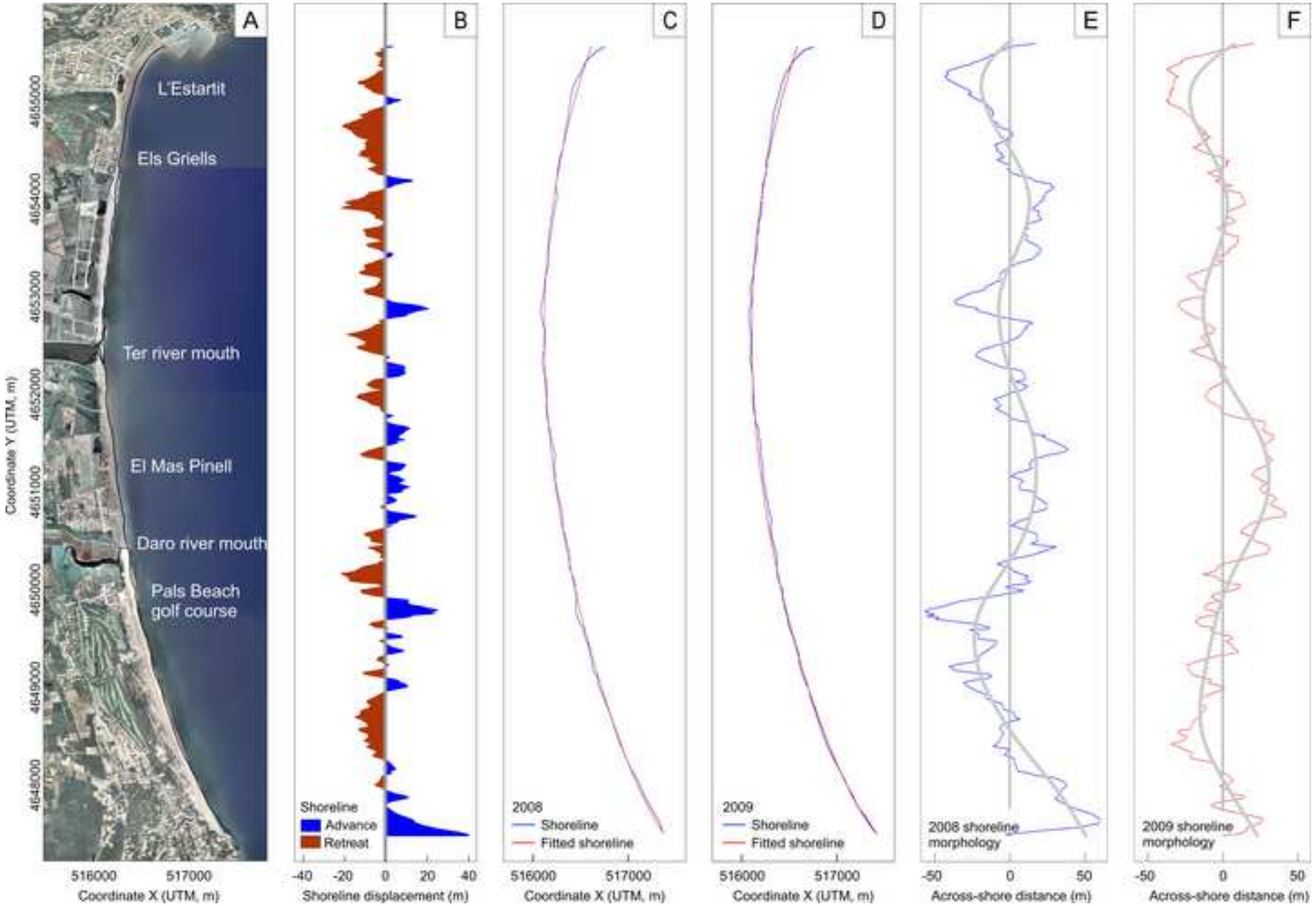

Figure (Color)
Click here to download high resolution image

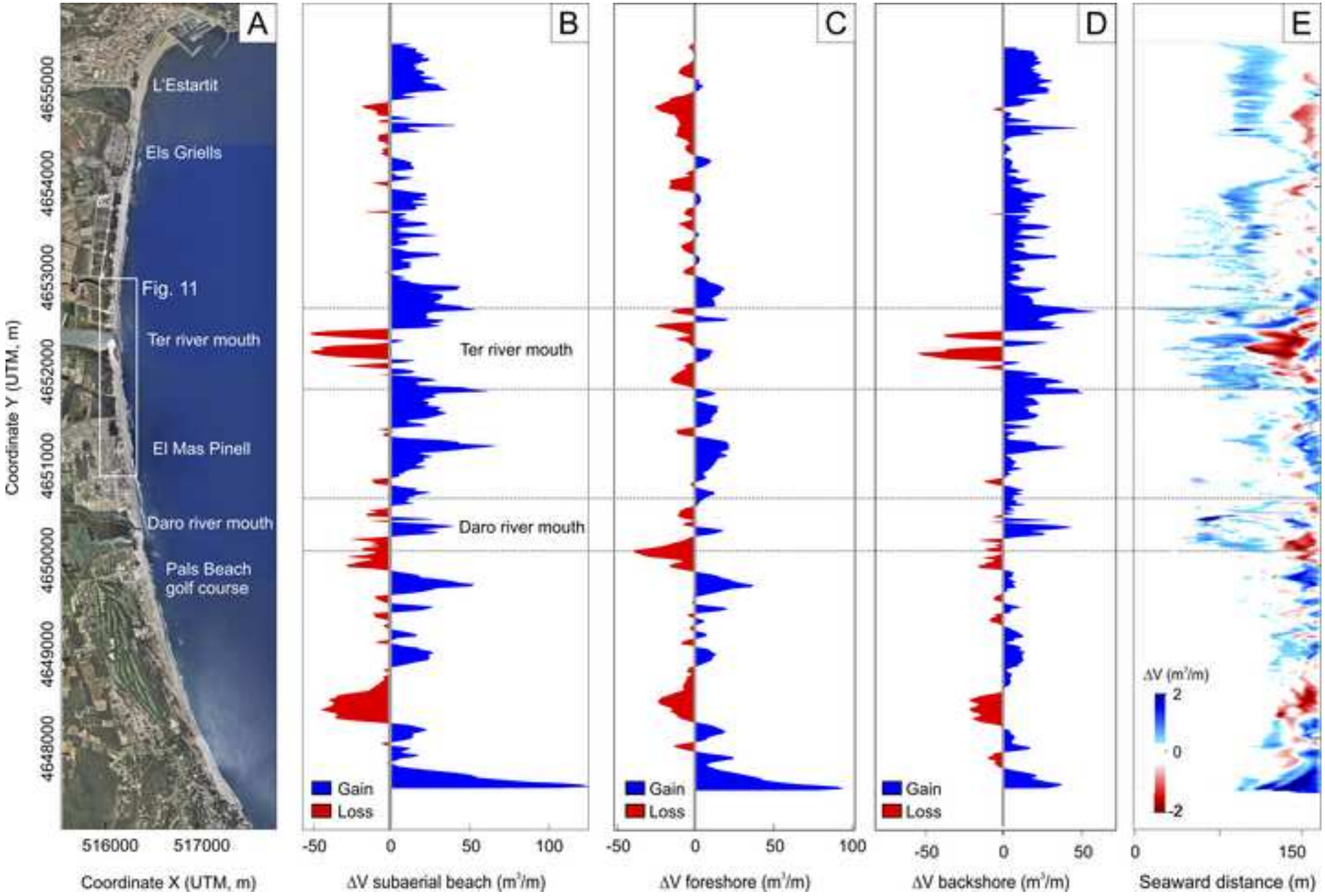

Figure (Color)
Click here to download high resolution image

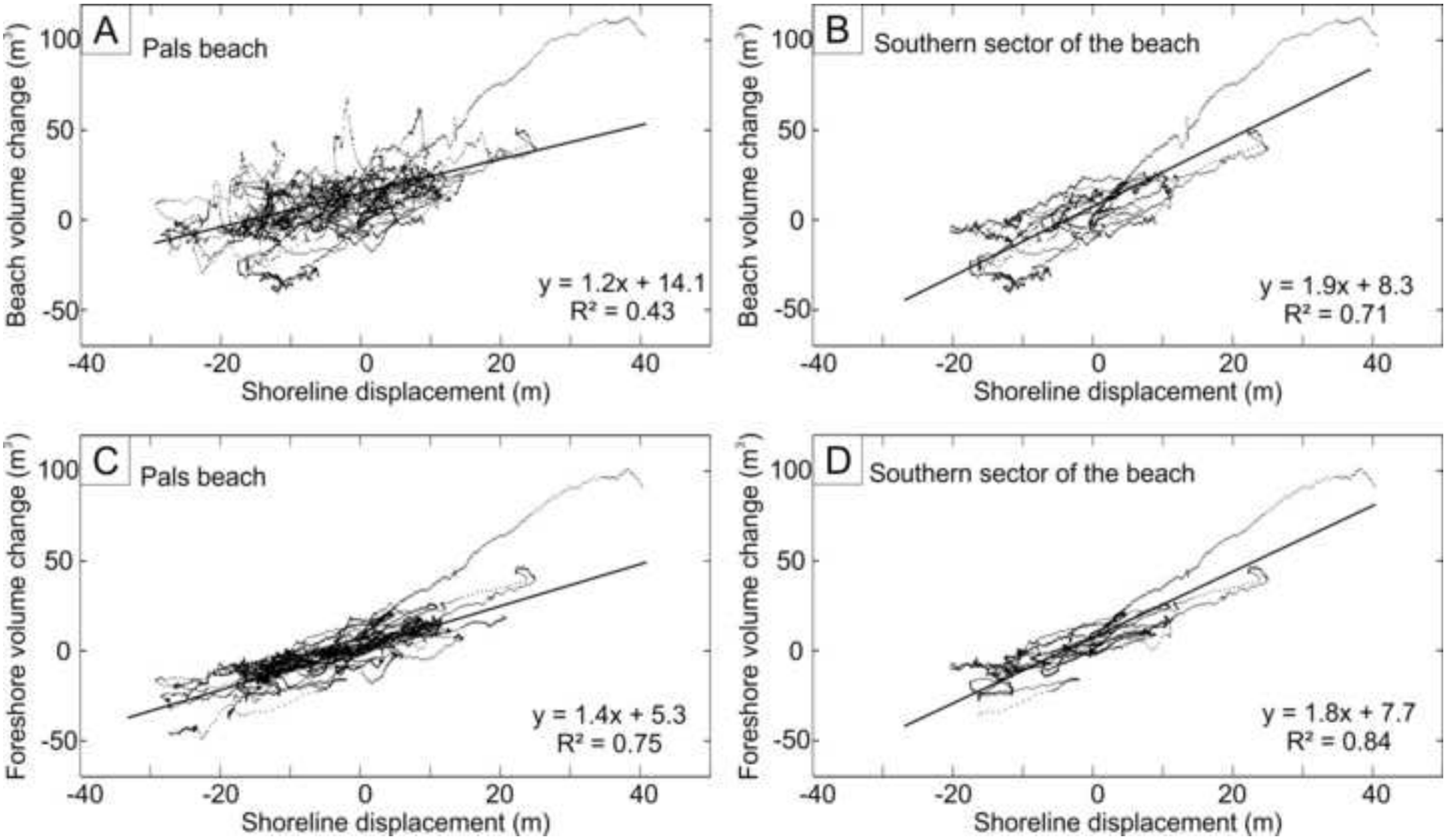

Figure (Color)
Click here to download high resolution image

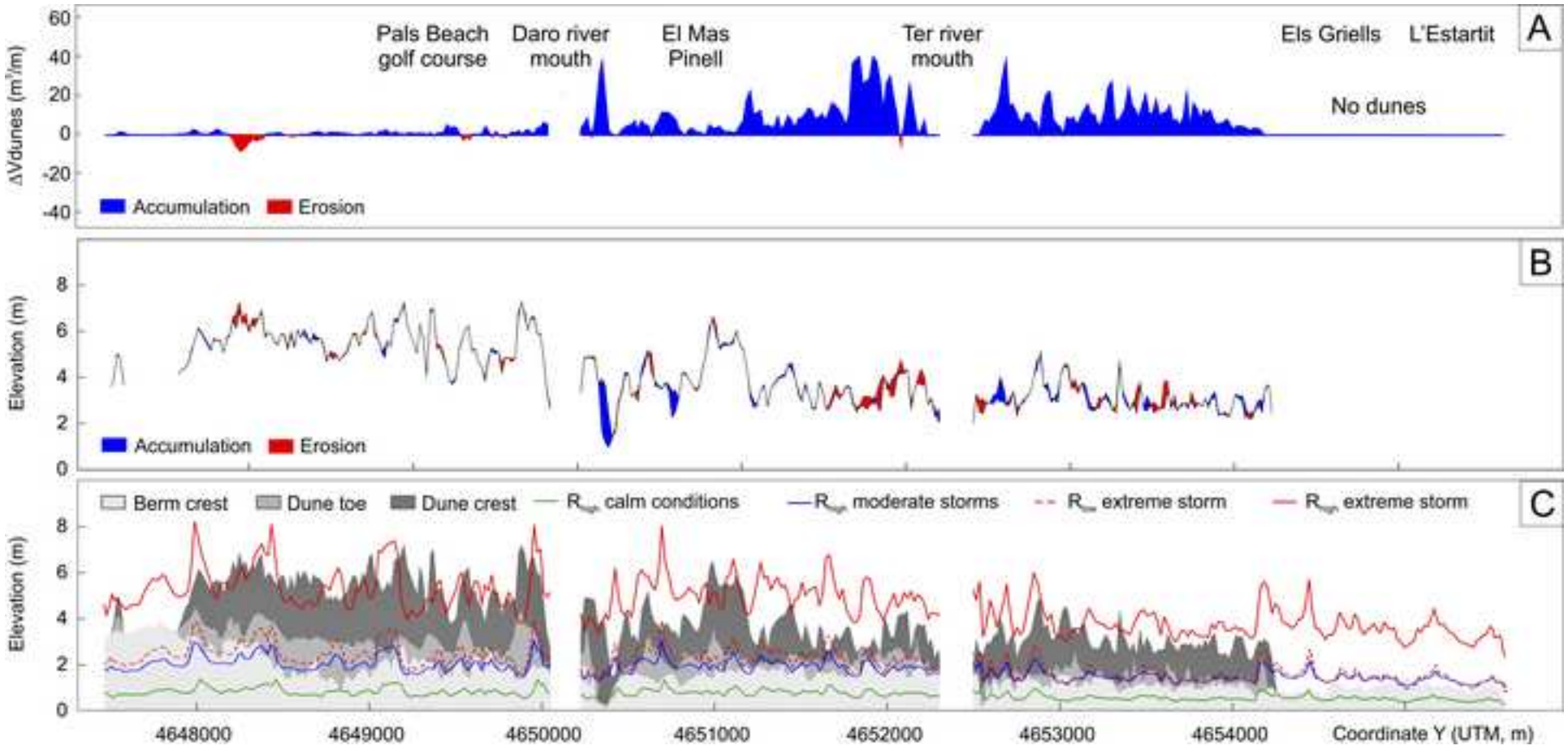

Figure (Color)

Click here to download high resolution image

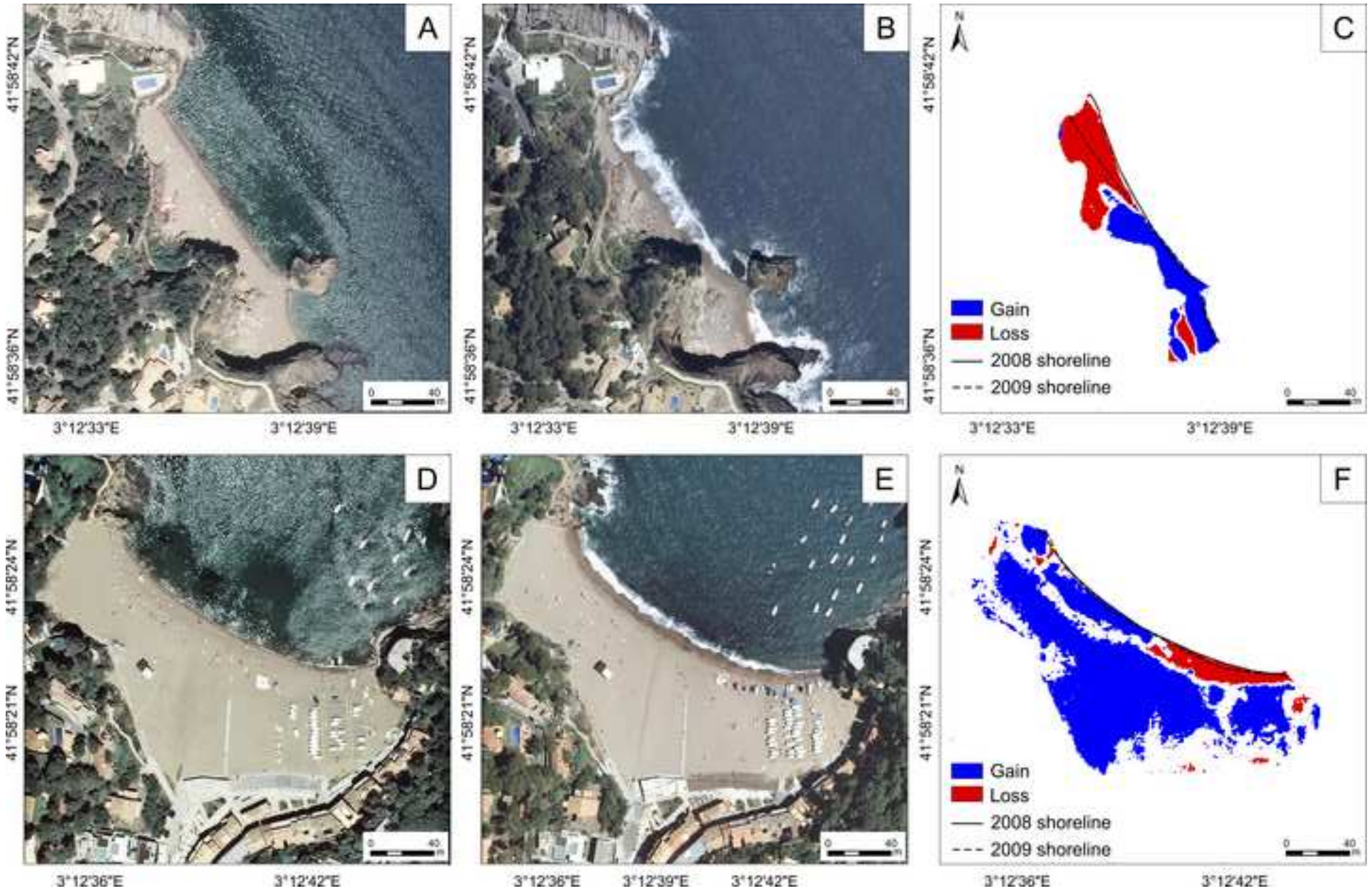

Figure (Color)
Click here to download high resolution image

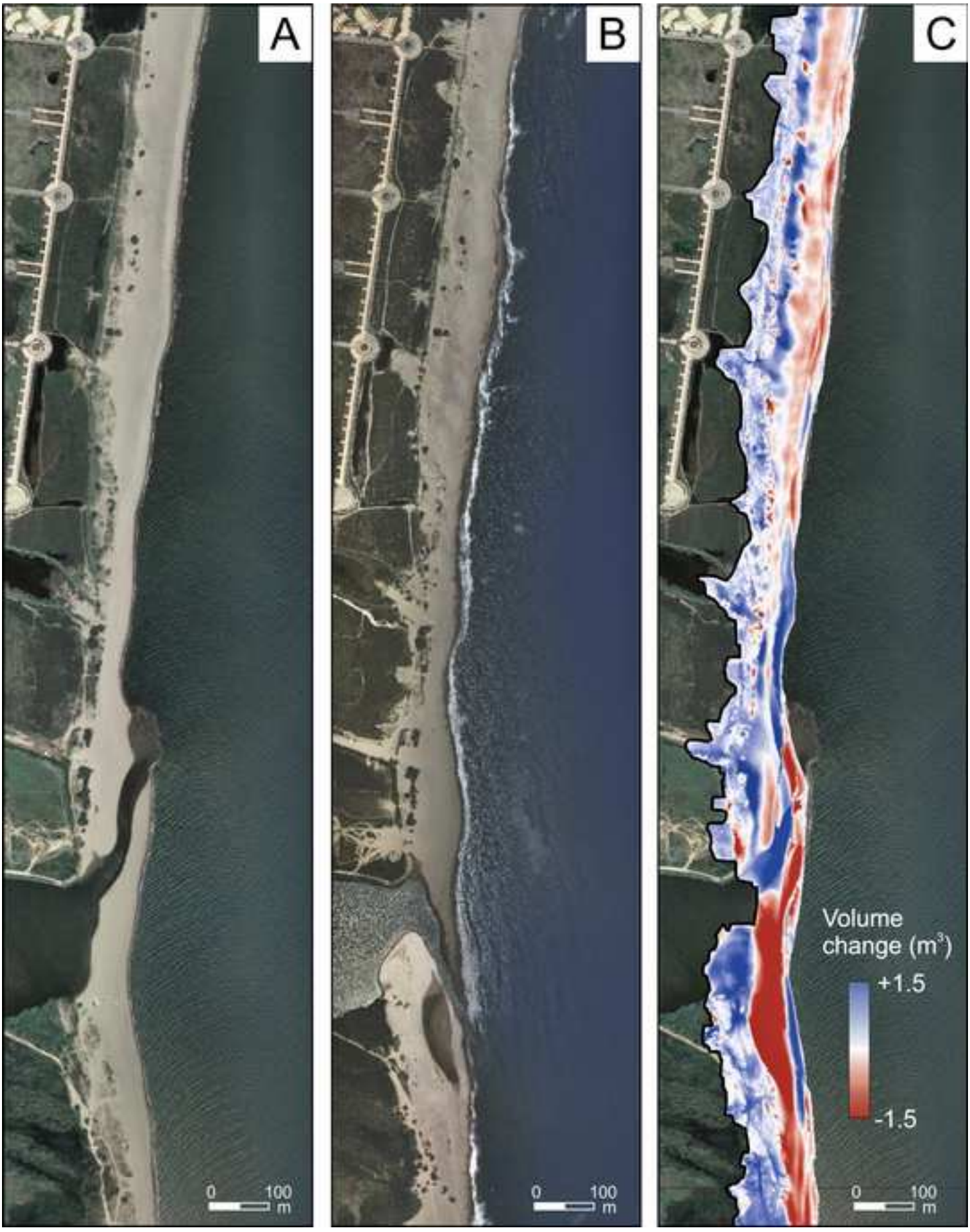

Figure (Color)
Click here to download high resolution image

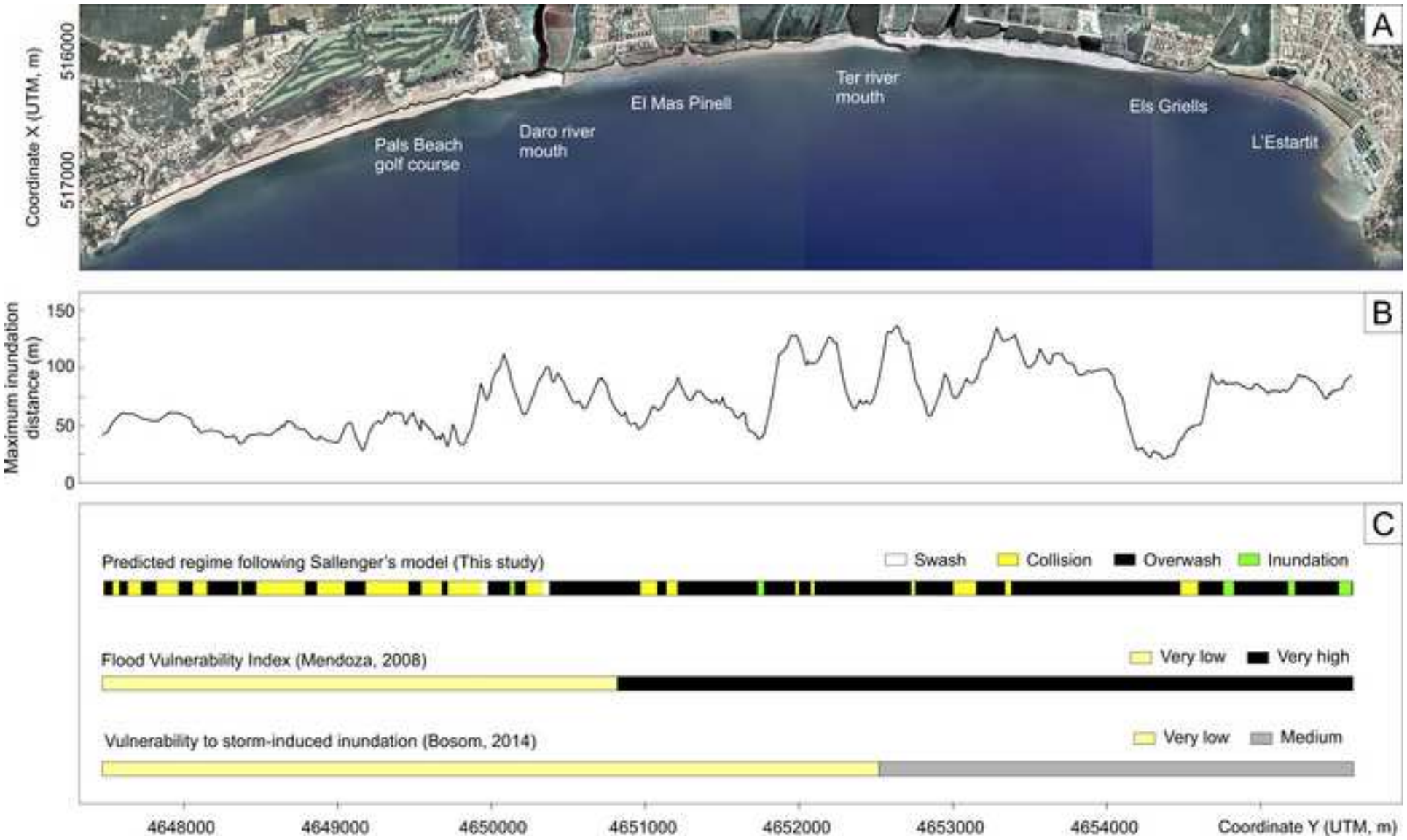

Figure (Color)
Click here to download high resolution image